The Influence of the Peduncle on Swimming Performance in Biological Tuna and Tuna-Inspired Artificial Propulsors

---

A Thesis

Presented to

the faculty of the School of Engineering and Applied Science

University of Virginia

---

in partial fulfillment
of the requirements for the degree

Master of Science

by

Gregory Thomas Lewis

May 2017

APPROVAL SHEET

This Thesis
is submitted in partial fulfillment of the requirements
for the degree of
Master of Science

Author Signature: _____

This Thesis has been read and approved by the examining committee:

Advisor: Hilary Bart-Smith

Committee Member: Dan Quinn

Committee Member: Haibo Dong

Committee Member: _____

Committee Member: _____

Committee Member: _____

Accepted for the School of Engineering and Applied Science:

Craig H. Benson, School of Engineering and Applied Science

May 2017

Abstract

Designers of unmanned underwater vehicles (UUVs) are increasingly turning to aquatic animals that use lift-based propulsion for inspiration. This is because of the significant advantage they have over traditional rotary propeller systems, such as efficiency and maneuverability. Thunniforms have been identified as fast, economical swimmers. If the performance of the next generation of UUVs is to achieve these biological performance metrics, it is essential that we understand and quantify the key mechanisms that contribute to their superior swimming performance. Significant efforts have been directed toward quantifying the morphometrics, kinematics, and material properties of thunniform swimmers. Through careful dissection, it was observed that the peduncle region of tuna and tuna-like fish allows for a degree a freedom. This motivated studies of the biology and artificial propulsors to quantify the role this subsystem has on speed, work done, and economy. Results show that the peduncle joint significantly improves performance: boosting speed and decreasing power compared to a fish without it and was reproduced in an artificial tuna-like platform. Additionally, modulating the joint stiffness and bend angle has profound effects on performance with preferred kinematics depending on swimming speed. These findings can inform the tail design of a high-performing UUV based on the biomechanics of a tuna.

Acknowledgments

I would like to thank all the people who have ever worked with me in the lab—Sean, Marianna, Darius, Aaron, Carl, and anyone else—for making the past six years an enjoyable time. Thank you to Samane for providing guidance (and many laughs) over the years. I would like to thank Trevor for teaching me a whole lot of things (and everything else he did for me). Thanks to Vishaal and Roger for all their help and support. Thanks to Dylan Wainwright and the rest of Lauder Labs for helping with the biological information and providing samples. Thanks to Dani, Kelsey, Will, and Frank of the Liquid Life Lab for being great people to work with. Thank you to Haibo Dong and the rest of the Flow Research Simulation Group for all their help. A huge thank you to Joe who has been there every step of the way and who was always willing to help, talk, or do whatever I asked. Lastly, I'd like to thank Hilary for giving me the opportunity to work in the lab first as an undergraduate and then as a graduate student. I am extremely grateful for the experience and all her support over the years.

List of Figures

Nomenclature

τ_i	Instantaneous torque
P_i	Instantaneous power
ω_i	Instantaneous angular velocity
θ_i	Instantaneous angular position
dt	Time step
$\bar{P}$	Cycle-average power
ξ	Economy
U	Free-swimming velocity
St	Strouhal number
f	Flapping frequency
A	Tip amplitude

Contents

Chapter 1
Introduction

In recent years, developers of unmanned underwater vehicles (UUVs) have become increasingly interested in the non-traditional propulsive mechanisms that are displayed in biology (Colgate and Lynch, 2004; Bandyopadhyay, 2005). Lift-based oscillatory swimming of animals such as tuna, rays, and dolphins could provide significant advantages over traditional rotary propeller in terms of speed (Aleyev, 1977; Fish and Rohr, 1999), maneuverability (Fish and Rohr, 1999), and stealth (Moulton, 1960; Kasumyan, 2008). Perhaps the most important benefit conferred by lift-based propulsion is in improvements in economy and efficiency, significant in particular to autonomous underwater vehicles (AUVs) whose purpose often involves long missions with little or no opportunity to refuel or recharge. In addition, these animals often display more than one of these characteristics at once, for example, being highly maneuverable while swimming very quickly. This stands in contrast with UUVs which are often optimized for one purpose: a long, sleek, torpedo-like, propeller-driven vehicle designed for speed, but not very maneuverable vs. a smaller, easily steerable, but comparably slow design. Biologically-inspired designs could not only span the performance gap but outperform current vehicles at both extremes, and parties such as the U.S. Navy have made their interest in such research clear.

Previous studies have examined ray-like swimming in this context (Moored et al., 2011; Fish et al., 2011), but tuna—which also display all of the aforementioned qualities—are an equally

promising candidate. These fish are highly-specialized for fast, economical swimming in the open ocean, but the fundamental science underlying their locomotion is not well understood. The complicated morphology and kinematics of these animals enable the desirable characteristics of their swimming, but also creates a system that is difficult to analyze and reproduce artificially. It becomes necessary to deconstruct the whole swimming mechanism to better understand the contribution of each constituent part. The peduncle region of tuna is of particular interest because it acts as a hinge between the body and the caudal fin, in effect giving a degree of freedom to an otherwise inflexible system. The overarching goal of this work is to investigate and quantify the role that this degree of freedom at the peduncle plays in the swimming performance in tuna, towards the goal of creating a high-performing artificial peduncle.

There are two main objectives pursuant to that goal. The first is to quantify the effect that the degree of freedom located at the peduncle has on swimming performance in tuna. This has not been previously measured and is important in order to confirm whether the peduncle has any effect at all, though it almost assuredly does. After establishing its relevance, the second is to vary the characteristics of the peduncle and thus determine the sensitivity of swimming performance to such parameters. This informs on the optimal configuration for an artificial peduncle, as well as provides insight back into the biological mechanism.

Chapter 2 provides a brief biological framework for understanding the goals of this work, along with a review of important and current studies into oscillatory swimming mechanics. Chapter 3 details the programs and instrumentation used across all the experiments. Chapter 4 presents the results and discussion of the first objective, while Chapter 5 does the same for the second. Lastly Chapter 6 summarizes the major findings, draws conclusions, and presents opportunities for future work.

Chapter 2
Background

2.1 Internal Biology

Tuna and mackerel together comprise about 15 species of the family *Scombridae* and share several key internal and morphological features that distinguish them from other fish, and many of these differences are what enable them to be such high-performance swimmers. Tuna are notable for their increased red muscle mass—the aerobic muscle fiber responsible for sustained swimming—and white muscle which has been modified to increase its aerobic capacity (figure 2.1). The red muscle has also moved to the core of the fish, which leads to a second peculiarity. Many tuna are endothermic, and the internal red muscle, together with a network of counter-current exchanging blood vessels, helps to generate and retain heat. This adaptation helps conserve energy in these animals which already have a higher metabolic cost than most other fish. Tuna also use a modified muscle to heat their eyes and brain, two of the most metabolically expensive organs. Another distinguishing feature is the structure of the scales, which are thickened and plate-like. A cross-section of the scales reveals that they are largely hollow, with struts of bone crossing throughout, and filled with fat (figure 2.2). Although there is no accepted explanation for the function of these modified scales, it is hypothesized that they aid in the conservation of heat by providing insulation.

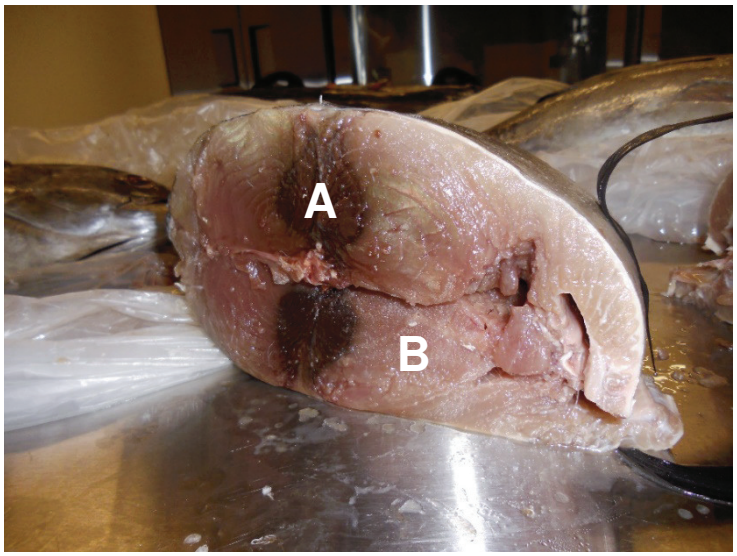

Figure 2.1: The cross-section of a tuna taken during a dissection at Lauder Labs in 2015. A) Large cores of red muscle close to the center of the body; B) Modified white muscle.

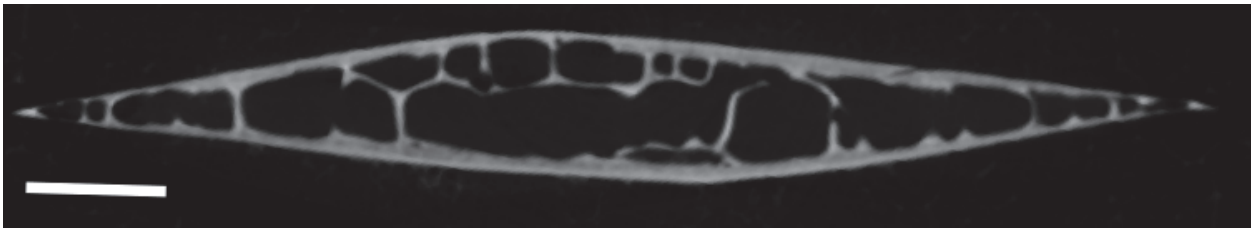

Figure 2.2: A cross-section of a tuna scale showing its largely hollow inside crossed by many bony struts. The scale bar represents 1 mm. Provided by Lauder Labs.

Tuna also possess a unique skeletal structure. Describing their backbone, Kishinouye (1923) notes that their "vertebrae are articulated together so firmly that the vertebral column allows little motion to either side. The free lateral movement of the vertebral column is possible only at the root of the caudal fin," i.e. the peduncle. These vertebrae are both smaller and irregularly-shaped compared to the rest of the spine, and there are several close together to allow for articulation

(figure 2.3). The last few non-caudal vertebrae have a few peculiarities as well. The neural and haemal spines actually

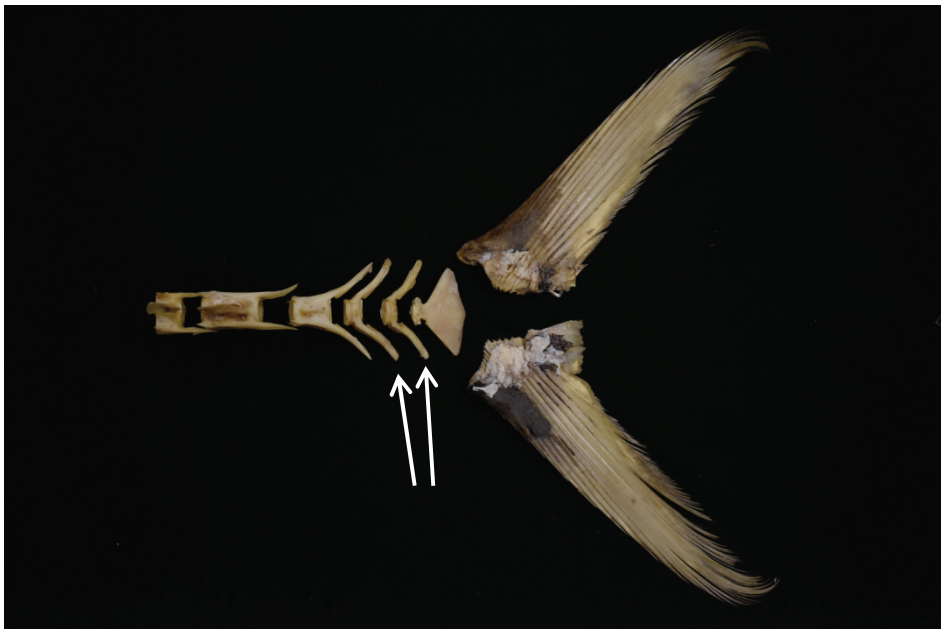

Figure 2.3: The skeletal structure of the posterior of an albacore tuna. The arrows designate the two narrow bones which allow the peduncle to rotate.

bend over to interlock with the next bone. They also have two flat projections from each side called a keel. Both of these further limit lateral motion.

The structure of the peduncle is almost entire skeletal. There are no muscles within the peduncle itself, but only tendons which span it to connect the red muscle in the trunk to the attachment points at the base of caudal fin. There are five major tendons on each side: the great lateral tendon, two lateral tendons, and a second pair of minor lateral tendons (figure 2.4). In addition, there are posterior oblique tendons which have numerous attachment points along the spine. These were noted during tuna dissections carried out at Harvard University in 2015. The joints at the peduncle rotate with little resistance though the tendons, skin, and other tissue provides the area some stiffness, but the skeletal structure does create a hard mechanical stop at the limits.

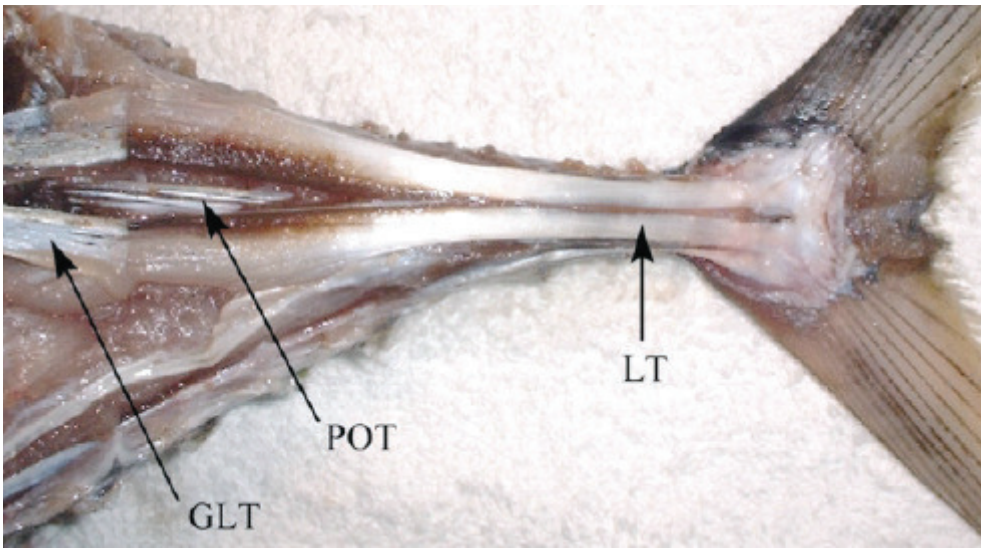

Figure 2.4: A dissection of a yellowfin tuna showing the great lateral tendon (GLT), lateral tendons (LT), and posterior oblique tendons (POT). The second pair of lateral tendons is not visible. From Shadwick et al. (2002).

2.2 Kinematics and Morphology

Tuna belong to a class of fish locomotion termed "thunniform" swimming. Each class designation relates to the percentage of body length which is prone to horizontal motion during swimming. Anguilliform swimmers, such as eels and lampreys, create a large flexion wave along the majority of their bodies; with each subsequent class—sub-carangiform, carangiform, and then thunniform, that wave becomes more and more limited to the back of the fish. Thunniforms concentrate their flapping motion in the back third of their body with very limited head movement and body wave (figure 2.5). This form of swimming appears not only in tuna but in other species that are known to be fast and economical, such as dolphins and orcas. Though visually very different, tuna and these odontocetes share several morphological characteristics. They both have a fusiform (spindle-shaped) body connected to a large, stiff, lunate caudal fin by a narrow peduncle region. The peduncle allows bending between the body and the caudal fin.

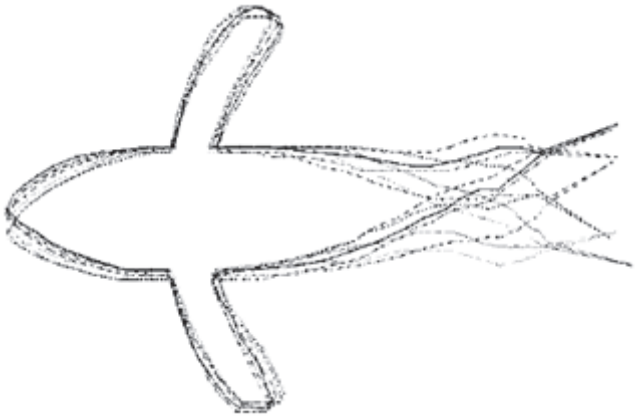

Figure 2.5: A drawing illustrating thunniform swimming kinematics. Most of the motion is in the tail of the fish. From Dewar and Graham (1994).

In addition to the body-scale kinematics, each of the fins displays its own kinematic patterns. Tuna can be observed deploying and retracting their pectoral fins and first dorsal fin during swimming as an aid in maneuvering. These fins fit into special pockets when folded in as not to interrupt the sleek profile of the fish. Tuna also possess small finlets running from their second dorsal fin and anal fin down to the peduncle. Despite their small size, they are individually controllable and are thought to further assist in maneuverability or to impart some desirable characteristics to the flow field. Though the caudal fin is largely inflexible, both spanwise and chordwise deformations can be observed during swimming, which is also thought to improve performance (figure 2.6).

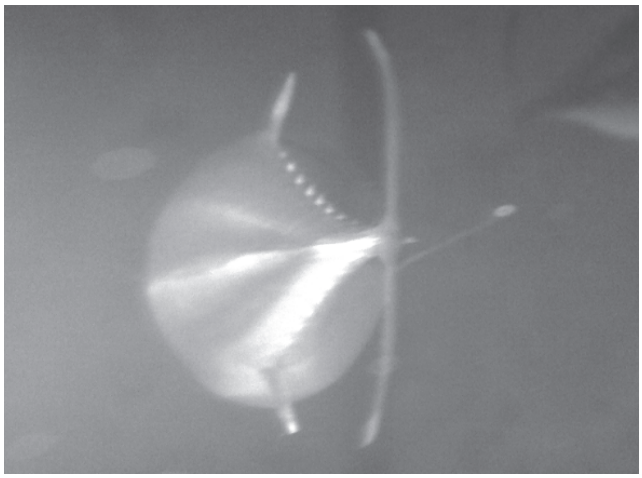

Figure 2.6: An image showing deformation at the tips of the caudal fin of a tuna. The finlets are also visible. From a video provided by Lauder Labs.

2.3 Summary of Biology

Each of the above adaptations reflects the specialization of tuna. Their biomechanics are extremely well suited to their lives in the open ocean, and many aspects of their behavior reflect that. The muscular and circulatory modifications that retain heat help them conserve energy while they dive to hunt. Their increased red muscle makes them excellent distance swimmers, migrating across oceans to live and breed. In short, tuna are designed to be exceptional swimmers, and they swim at higher average speeds because of it. It is, however, costly, and many of their adaptations also show efforts to conserve energy. Thunniform locomotion is likely economical for this very reason, and even within the framework of thunniform locomotion, the peduncle is unique. Due to the limited body movement inherent in thunniform swimming and the stiff caudal fin, the peduncle's ability to bend significantly is striking, motivating this work.

2.4 Theoretical Framework

While the goal of this work is to investigate the role of the peduncle, the concept of stiffness has been the guiding principle throughout the entire process of design and experimentation. The initial foray into a stiffness-based rationale stemmed from a desire to map the stiffness of dolphin flukes. A rig was built consisting of a load cell attached to the end of a linear actuator, which was then mounted on an x-y stage (figure 2.7). This device would "poke" a fluke at many points across its surface while measuring load and displacement. From this data, flexural stiffness values could be calculated, creating a spatial map of stiffness for the given fluke. This process was done initially with an artificial dolphin fluke (figure 2.8). This system was then used on a tail of a real tuna sample, where only values at several points along centerline were measured in order to gauge the stiffness of the peduncle. While the stiffness values from this test did not directly influence later experiments and the endeavor ended up being more of a thought experiment than a long-term project, it was important in that stiffness then became the lens through which much of this research was viewed.

Many others have also used stiffness as the basis for investigating swimming performance. Feilich and Lauder (2015) studied the effects of peduncle and caudal fin shape and flexibility with tuna-inspired passive heaving foils, observing the complex interactions of stiffness and shape even

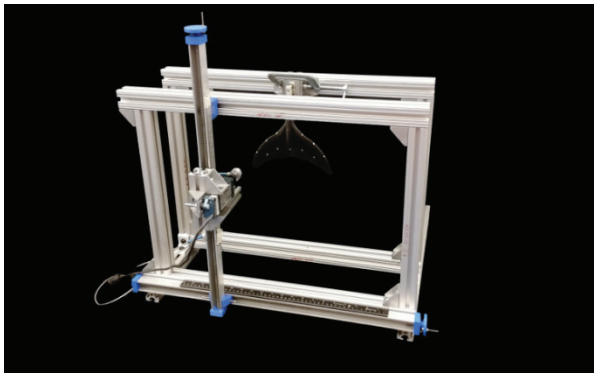

Figure 2.7: The poking rig with an artificial fluke mounted in the device.

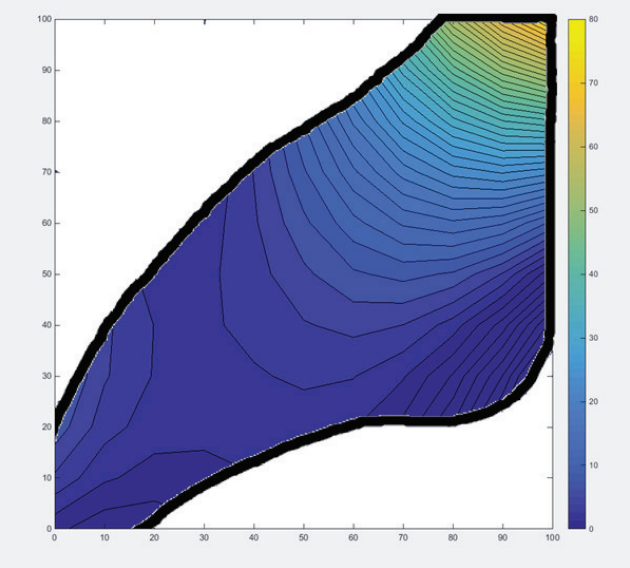

Figure 2.8: The positional map of flexural stiffness for an artificial fluke.

in their simple models. They note the potential of the phase relationship between the body and tail as an indicator of swimming performance, and point out that it may not be ideal to study tails in isolation because of these flow interactions between the body and tail. Lucas et al. (2015) and Rosic et al. (2017) also investigated stiffness in tuna-inspired foils. The former used non-uniform stiffness rectangular panels, while the latter used uniform stiffness panels shaped like a tuna caudal region. Both found a complex relationship between stiffness and swimming performance that were not always in agreement with other studies.

Dewey et al. (2013) showed that flexibility increased thrust over a rigid panel in pitching experiments. The power input to the fluid depended on several factors, but the overall efficiency always increased. However, stiffness was important in maximizing efficiency, and performance degraded if the panel was too flexible or rigid. Quinn et al. (2013) also found that flexibility increased economy in particular at slower swimming speeds in heaving experiments. In contrast, Shelton et al. (2012) found that stiffer panels performed better than flexible in many cases. Though

these are but a few of many studies on stiffness's role in swimming, it is clear that there is not a hard-and-fast rule to determine performance based on stiffness in these simplified models.

Other studies have explored stiffness in dolphins, both in their peduncles and flukes. Park and Cho (2013) laid out the design for a robust, variable stiffness artificial peduncle based largely on work of Sun et al. (2010), who examined the structure and measured the bending properties of a dolphin peduncle using tendon actuation. Park et al. (2014) went on to test this structure and found that as frequency increased, a stiffer peduncle increased thrust production.

As highlighted by Feilich and Lauder, stiffness affects the phase delay, and some have chosen to bypass passive stiffness models and control the phase directly. Esposito et al. (2012) built and tested a robotic fish tail based on the motion of a bluegill sunfish with individually controllable fin rays. They found that varying the phase and motion profile of the fin rays changed the force production and flow structure. Ren et al. (2016) conducted a similar study with their own robotic sunfish and came to the same conclusions: phase delay could improve the mean thrust and lift as well as the direction of vortex shedding. They go on to hypothesize this second result could indicate the use of vectoring as an aid in maneuverability.

Shadwick et al. (2002) conducted tests on tuna tendons to determine internal structure as well as mechanical properties. Blickhan and Cheng (1994) found that elastic tissues, such as tail tendons, in cetaceans stored energy and reduced energy cost during swimming. Whether such a mechanism was present in tuna had not been researched. Shadwick et al. found that based on the mechanical properties of tuna tendons and the loads present during swimming that they did not serve a purpose in energy storage.

The above studies provide a solid foundation for this research, but there are several areas where it can fill in gaps. This work intends to:

- Investigate the performance role of the peduncle of tuna, using biological samples and tuna-like artificial propulsors

  The studies on peduncle stiffness and phase relationship do not study tuna but rather other slower or less economical fish or dolphins. Nor have any tests been done to evaluate the influence of the peduncle on performance using biological tuna samples in an experimental setting. Based on the planform stiffness assessment, it is hypothesized that the peduncle plays a significant role in swimming by introducing an extra degree of freedom to the kinematics. To this end a series of tests to isolate the peduncle and probe the extra degree of rotational freedom it allows.

- Increase the complexity of the passive caudal and peduncle models by including biologically-relevant structures and a tuna-like body platform.

  The simplified panel models do a good job of illustrating the complexity of the topic and provide some general guidelines concerning stiffness and performance. The aim is to step the experimental models closer to the biological structure to observe whether the same trends appear. Flexible foils will be replaced by a hinge joint and an aerofoil-planform caudal fin. Additionally, the tuna-like panel studies note the difficulty of testing fins in isolation. This work also increases the realism of the experimental setup by including a tuna-like body platform. It is hypothesized that increased flexibility will improve performance even in these more complex and more biofidelic systems.

- Determine whether the engineered artificial propulsors can achieve performance on par with biological fins.

  The aim is to see whether engineered solutions to biological problems can still faithfully reproduce the kinematics and performance. There are also opportunities for improvement of biological design. Tuna tendons do not seem to act as an energy storage mechanism even at maximum effort. If the tendons are modeled using springs in this passive peduncle model, can the kinematics be reproduced with energy savings? It is hypothesized that the artificial peduncle is capable of performance equal to and even better than a biological fin.

It should be noted that this work is only concerned with the effect that the degree of freedom at the peduncle has on swimming performance. When it is stated that the "role of the peduncle on swimming performance" is to be investigated, what is meant is that the "role of the degree of freedom located at the peduncle" is to be investigated. The abbreviated form is used for the sake of concision. Other features of the peduncle, such as the sudden narrowing or the unique shape, could also affect performance, but any reference to the "role of peduncle" in this work specifically refers to the role of the degree of freedom located there.

Chapter 3
Experimental Setup

Free-swimming tests were carried out on tuna and mechanical platforms to understand and quantify the role of the peduncle on swimming performance. All of the following performance tests utilize the same equipment and a very similar test procedure, which will be outlined in the following sections. Any deviations from the general experimental setup will be addressed in the relevant chapter. Data on free-swimming speed and power was recorded in real time for the various propulsors. A custom-built rig to approximate free-swimming conditions and a flow tank were necessary to accomplish this, as well as the program that operated the rig and collected the data. In addition, a tuna-like platform was developed for the artificial propulsors to increase the bio-authenticity of the tests. Once collected all data was processed in a separate program.

3.1 Equipment

3.1.1 Flow Tank

Every test took place in a recirculating water tunnel, i.e. "flow tank," a Model 1520 water tunnel from Rolling Hills Research Corporation. The tank is capable of producing speeds up to 36 in/s (about 0.9 m/s) with turbulence of less than 1% RMS. Flow speed is manually set with a resolution of 0.1 in/s (2.54 mm/s) and is controlled by a calibrated flow meter located in the return

pipe. The test section of the tunnel measures 15 in (38.1 cm) wide, 20 in (50.8 cm) deep, and 60 in (152.4 cm) long. Glass construction and a window at the rear allow the side, bottom, and back of the test section to be viewed, making it easy to film multiple angles for kinematic data. The flow tank also has second optional return pipe which routes through a sediment filter, which helps clean the tank clean when testing biological samples. The flow tank is also fitted with a wave suppression panel which sits just below the water's surface.

3.1.2 Test Rig

Every test also a specially designed "test rig," which has three main requirements. It approximates free-swimming conditions, actuates the propulsor, and collects the desired measurements. The free-swimming condition is accomplished by having the rig glide on two frictionless air bushings (New Way Air Bearings) riding along two 18-inch long, half-inch cylindrical steel rails (McMaster-Carr). Two onboard tanks of nitrogen pressurized to a maximum of 4500 psi supply the bushings with a regulated pressure of approximately 75 psi; both tanks at maximum capacity provide enough nitrogen to run the rig for about 35 minutes. The actuation of the propulsor is achieved with a Dynamixel MX-64 servo (Robotis), a "smart servo" that can provide position, temperature, and voltage feedback information in addition to normal servo function. A torque sensor is attached to the motor to measure mechanical power input torque data, and a custom-milled aluminum coupler joins the sensor to the drive shaft of the propulsor. The torque sensor is a TQ202-25 (Omega) which can measure ±25 in-lb (±2.8 N-m) of torque with a stated accuracy of 0.2% of the full-scale output. Torque data is collected with a custom-built instrumentation amplifier and a USB-6009 DAQ (National Instruments), and a LabView program controls the operation of the whole system. The motor, DAQ, and amplifier are powered using two

off-board power supplies. All signals to and from the rig run through extremely flexible cable suspended overhead with enough slack as to not affect the rig's motion in any way. Figure 3.1 shows a schematic of the rig and signal flow. The rig is able to test up to 3 Hz for most propulsors. After 3 Hz (and at 3 Hz for certain fins), the rig vibrates. This causes the bushings to lock up and provides inaccurate results for speed.

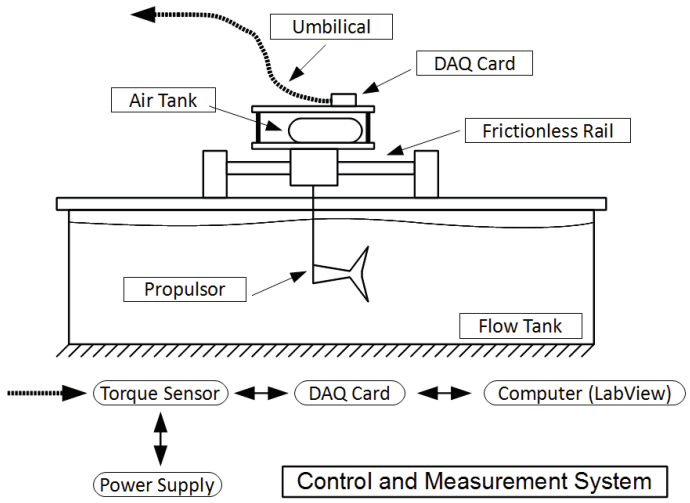

Figure 3.1: A schematic of the rig highlighting the important features of the system.

3.2 Experimental Procedure

The test procedure is as follows. After ensuring the propulsor is in a proper neutral position with respect to the incoming flow, the test is started and the propulsor begins to swim forward. Once it reaches the front of the rig, the flow speed is slowly increased until it settles with no (or very small) oscillations about the center point of the rails. This is assumed to be steady-state swimming, and torque and angular position are then recorded over several cycles; final swimming speed is also logged. This process is repeated over the range of relevant frequencies as one set of tests. Multiple sets of tests were conducted to obtain mean values and standard deviations, but the specific number

varied. For one set of tests, videos were recorded to obtain kinematic data and tip amplitudes for Strouhal number calculations; these videos were taken as representative of every test at that frequency. This is used for both sets of peduncle experiments, only the propulsors differ. Tests are run at constant amplitude over a range of frequencies. Though the specific frequency range differs for each propulsor depending on the size of the fin and at what frequency each fin begins to produce thrust (i.e. smaller fins would not swim at very low frequencies), the total range for all tests is 0.5 to 3 Hz. All tests use a symmetric sine wave motion profile.

3.3 Post-Processing and Calculations

The data output by the LabView program was processed in a separate MATLAB script to calculate swimming performance. In all tests, instantaneous mechanical power, P_i, is calculated as the product of instantaneous torque, τ_i, and instantaneous angular velocity, ω_i. Angular velocity is the derivative of the measured servo position with respect to time, calculated here according to the forward finite-difference method, $\omega_i = \frac{\theta_i - \theta_{i+1}}{dt}$. For each test, the mean power is calculated by averaging all the instantaneous powers over the test duration (number of samples), $\bar{P} = \frac{\sum P_i}{n}$. The free-swimming economy is calculated as:

$$\xi = \frac{U}{\bar{P}}$$

Where U is the free-swimming speed. Economy is used extensively in literature and provides a measure of distance traveled per unit energy (m/J in SI units). Note that efficiency, while also an acceptable measure of performance, requires thrust to be known, and is thus not conducive to these tests given the free-swimming condition; economy is the more appropriate choice.

Strouhal number is a non-dimensional frequency that describes wake vortex shedding, and is often used in describing oscillatory lift-based swimming. Triantafyllou et. al (1993) found that the highest efficiencies fall in a range of Strouhal numbers from 0.25 to 0.35, which coincides with a wide variety of swimming animals. Strouhal number is defined as:

$$St = \frac{fA}{U}$$

Where f is the flapping frequency and A is the tip amplitude. Because the nominal frequency for each experiment was constant over the frequency range, the actual amplitude decreased as the frequency increased. The amplitudes for each test were instead acquired from the videos using Adobe Photoshop to measure the tip-to-tip amplitude for a given flapping cycle. This amplitude was then taken as representative for any tests with those given parameters (fin/peduncle and frequency).

Speed, power, economy, and Strouhal number are the four main metrics of interest, and are used to understand the performance of each fin, and thus the role the peduncle plays in its performance.

Chapter 4

Experiment: Biological Samples

The purpose of these experiments was to quantify the effect of the peduncle in biology. This was accomplished by comparing performance results between tests where the peduncle is allowed to rotate freely and control tests where the joint has been constrained to allow no rotation.

4.1 Experimental Setup

A total of five tails of four different species were tested: an albacore tuna, two bigeye tuna, a Spanish mackerel, and a yellowfin tuna (figure 4.1). Test samples were chosen from a larger batch of fins according to their condition, and so that the role of the peduncle could be assessed in a range of sizes and species. The lengths of the samples (measured from the truncation point to the center of the trailing edge of the caudal fin) ranged from 61 mm to 116 mm, and the spans of the caudal fins ranged from 111 mm to 340 mm. The fins were tested in the following order, and will be referred to by their sample number from here on: larger bigeye, albacore, smaller bigeye, yellowfin, and lastly the Spanish mackerel. In addition, the first two samples will be referred to as “the large fins” and the

last three will be "the small fins." The terms "sample," "fin," and "tail" will all be used interchangeably.

The samples were kept frozen when not in use and were thawed in cold water. The history of the samples with respect to being frozen, thawed, and refrozen is unknown before acquisition, but the thaw-refreeze cycles were kept to a minimum for the first two fins to minimize any effects that might have. Each of the last three samples was thawed, tested, and refrozen only once, so all tests occurred on the same thaw cycle, because of decomposition effects noted in the second sample.

Figure 4.1: The five tail samples used in the biological testing. From left to right, the species are: bigeye, albacore, bigeye, yellowfin, and Spanish mackerel. Fins 1, 2, 4, and 5 are shown mounted into their housings, and the strut used impose the constraint is visible in fin 1.

For testing, each tail was fitted into a custom drag body. For unconstrained tests, the tail was left untouched. For constrained tests, two different methods were used to limit the motion of the peduncle. For the first two samples, the constraint was imposed by attaching two light, low-profile struts to the sides of the tail. These were small enough that it was assumed they did not affect flow, moment of inertia, etc. outside of purpose to constrain the peduncle. For the last three samples, the tails were allowed to dry out in air for several hours, which hardened the peduncle, while leaving the properties of the caudal fin itself unchanged. This hardening was irreversible, and rehydration was not an issue. This method was simpler and more reliable than the struts, and thus preferable. The

last three samples are also considerably smaller than the first two, so the strut method would have been a questionable one for that reason alone.

After the above preparation, each of the five samples was tested according to the procedure outlined in section 3.2, with nominal prescribed amplitude of 30 degrees. Tip amplitudes of the unconstrained tests were measured using video analysis, as outlined above. The amplitudes of the constrained tests were calculated using trigonometry with the length of the fin and the angle of rotation.

4.2 Results and Discussion

The results of the tests show consistent trends across all five samples in each of the metrics of interest, presented below in figures 4.2-4.6. There are five key takeaways from the data. First and most importantly, the unconstrained tests consistently outperform the constrained tests. Second, there are speeds which optimize economy (figure 4.5). Third, many of the Strouhal numbers for the unconstrained tests fall in the range expected for optimal efficiency, but—fourth—Strouhal number is not a unique indicator of performance when using a free-swimming metric such as economy, (figure 4.6). Lastly, the trends between speed (figure 4.2) and power (figure 4.3) suggest a non-linear relationship between the two metrics. With these in mind, a more in-depth discussion follows.

Unconstrained Outperforms Constrained: Speed, Power and Economy

Figure 4.2 shows free-swimming speed plotted against flapping frequency. The unconstrained free-swimming speeds are consistently higher than those of the constrained tests. Both constraint conditions show similar trends: speed increasing with frequency but approaching a

plateau at higher values. Maximum speeds for each fin also correlate with fin size. More striking, however, is the difference between the powers of the constrained and unconstrained tests.

Figure 4.3 shows the average power plotted against frequency. The constrained peduncle always required more power than the unconstrained peduncle. For example, sample three swam at about 0.18 m/s at 2 Hz and required 0.2038 W in the constrained state. The unconstrained state for the same fin only required 0.03906 W to swim at the same speed—over six times less. The constrained tests consistently require 3 to 4 times as much power—and as high as 9.5 times as much—for the same frequency. The trends exhibited in the power data are considerably more varied than those that appear for speed, and they differ across sample and even between the constrained condition. Tails 1, 4, and 5 in the constraint conditions seem to indicate the same general trend as speed, increasing but seemingly approaching a plateau, but the rates are drastically different from their speed counterparts. Tail 3 shows a different trend entirely. The unconstrained tests vary almost perfectly linearly with frequency, while the constrained tests seem to show the power increasing at an increasing rate. Tail 2 seems to show a fairly linear relationship in both the constrained and unconstrained cases, but the slopes of each are very similar, unlike every other sample.

Figure 4.4 shows plots for economy vs. free-swimming speed. In all test cases, the unconstrained tails have a higher economy than the constrained tails, which is not unexpected considering the speed and power data. The constrained tests all show a similar trend with economy decreasing monotonically (in the case of tail 4 only very slightly) as speed increases.

Certain Speeds Optimize Economy

The unconstrained tests of the larger two fins exhibit peaks in economy, which occur at different frequencies (0.75 and 1 Hz) but very similar speeds (about 0.2 m/s), before monotonically decreasing. The unconstrained tests of the smaller fins do not show such behavior (likely due to

their small size and the limitations of the test system), and economy only decreases with increasing speed. The peaks in economy could be occurring because the fin is oscillating at some structural resonance, which causes similar peaks in economy in the work of Dewey et al. and Quinn et al. with flexible panels.

Strouhal Numbers fall in Expected Range, but the Metric is Not Unique for Economy

Figure 4.5 shows economy plotted against Strouhal number. Taylor et al. (2014) observed that most modes of lift-based oscillatory locomotion typically operate in a range of Strouhal numbers from 0.2 to 0.4. Many of the unconstrained tests do fall within this range, and some even fall below 0.2—perhaps normal given that these are truncated sections of dead tuna and not live animals. The unconstrained tests of the large samples do show significant banding, with a wide range of economies (about 0.6 to 1.4 m/J for the second tail) across a very narrow range of the Strouhal numbers (0.15 to 0.23). The band also occurs at the lowest Strouhal numbers. Many of the constrained tests for these samples show a similar trend, albeit shifted higher in Strouhal number and lower in economy. Fins 1, 2, 4, and 5 show clustering at the lowest Strouhal numbers, with economy actually increasing as Strouhal number increases. Fin 3 exhibits an uncharacteristic trend that is the mirror image of the expected shape, with a band at the highest Strouhal numbers. It is unsurprising that the constrained tests do not fall within the 0.2 to 0.4 range and display atypical trends because they are, by nature, "un-biological" compared to the unconstrained tests. The unconstrained tests for sample 4 are also somewhat atypical. Due to the corruption of the video files associated with these tests, the true amplitudes were unable to be measured. They were simply estimated using the same method as the constrained tests, which represents the upper limit of possible amplitude. The true amplitude decreases with frequency, which would result in lower Strouhal numbers and likely force the data into the "banded" trend like the rest of the samples.

It is interesting to note that maximum economy correlates inversely with fin size and that the lowest Strouhal numbers do not always correspond to the highest economies. Certain Strouhal numbers are often associated with high performance when using efficiency as a metric, but when using a free-swimming metric such as economy, Strouhal number does not uniquely correlate to high-performance, which is consistent with Kemp's (2014) results on batoid swimming and those of Quinn et al.

Non-Linearity Between Speed and Power

The considerable variation in trends between the speed and power data for each fin suggests a non-linear relationship between the two, and further analysis of some of the data substantiated this hypothesis. The constrained tests of power (figure 4.6) for samples 2 and 4 had consistently high standard deviations, which prompter further investigation. While there was no pattern in the results of tail 4 (the higher-than-normal standard deviations are perhaps a result of its small size), an interesting trend emerged in the data of sample 2. Figure 4.6 shows power plotted against frequency for sample 2, but instead displays the results of each individual test. The large variation in constrained power is not random. The results within each set of frequencies are consistent, but the power decreases with each subsequent set. The first (highest) set of data appears to be following earlier trends, with the constrained power several times higher than the unconstrained, until a sudden drop at 2 Hz. The following sets have lower and lower power, falling almost to the levels of the unconstrained peduncle. This likely represents a failure of the strut method to constrain this particular fin. There were no issues with the strut method in the other sample that utilized it (sample 1), and those results are unaffected. The inconsistency is in this test only, and no conclusions are compromised.

This particular sample, while still in good enough condition to be tested, had been frozen and unfrozen several times by the time these last tests took place, and more marked decomposition was starting to set in. The likely explanation is that the struts, which were initially tight against the surface of the tail, became loose at the higher frequencies because of the decomposing tissue. With each successive set, the strut loosened, and the imposed constraint was relaxed. Perhaps unsurprisingly, relaxing the constraint on the peduncle decreased the power to near the levels of the unconstrained tests.

What is surprising, however, is that there was no corresponding increase in speed. Although the power decreased markedly, the speed did not increase to the levels of the unconstrained tests. Combined with the observation of trends, this seems to suggest that speed and power are decoupled. Additionally, the "relaxing" constraint revealed another useful interaction: varying the "amounts" of constraint varies the performance. "Amounts" appears in quotations because the constraint of a degree of freedom is usually binary: it is free to move, or it is not. What constitutes an "amount of constraint" is open to interpretation. The next chapter is devoted to the investigation of this non-linearity and varying the constraints on the peduncle to tuna performance.

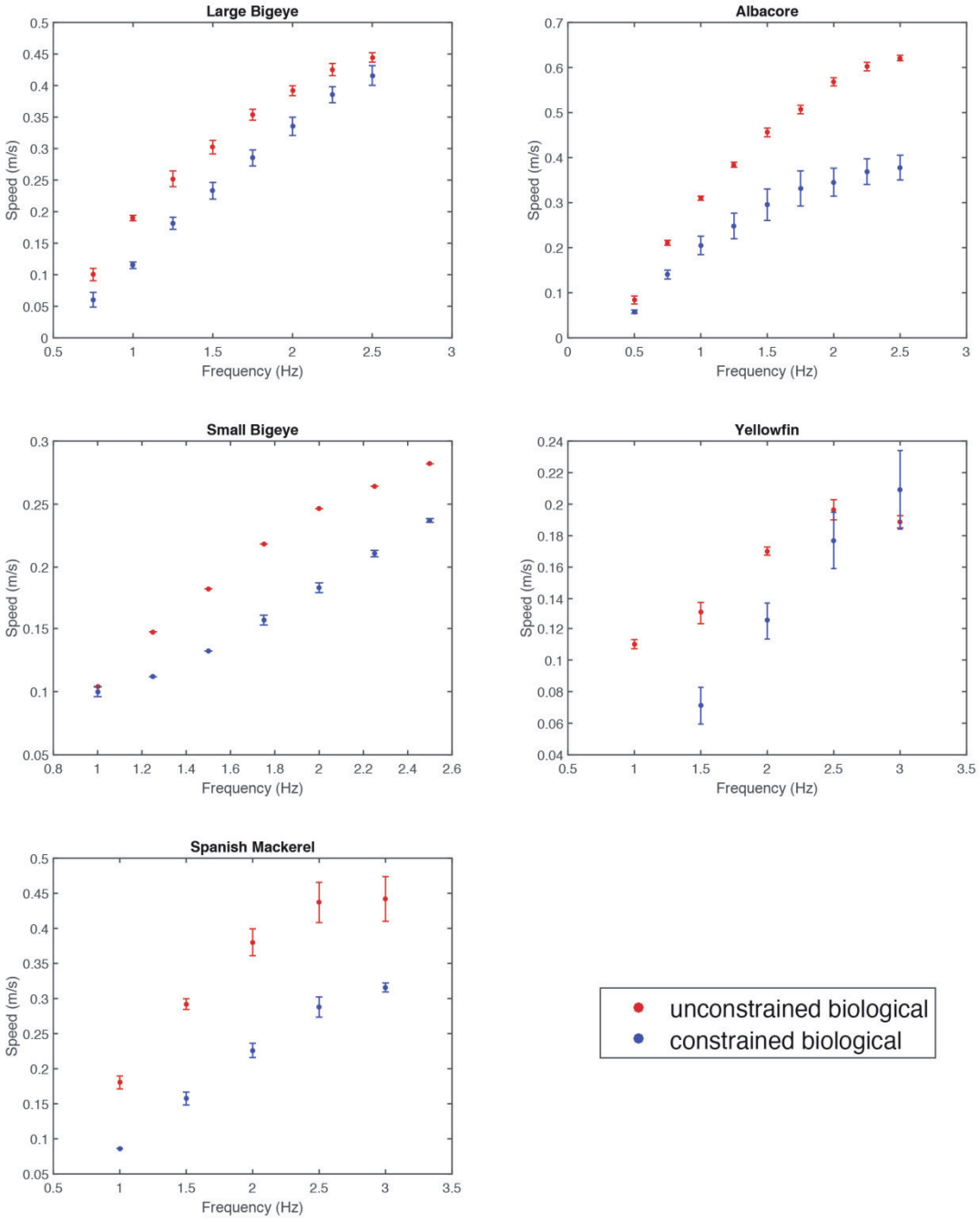

Figure 4.2: The results of free-swimming speed plotted against frequency. Error bars reflect standard deviations from the following number of tests: large bigeye: 4 tests for both constraint conditions; albacore: 4 tests for unconstrained and at least 3 for constrained; small bigeye: 1 test for unconstrained (due to an experiment error) and 3 tests for constrained; yellowfin: 3 tests for both; Spanish mackerel: 3 tests for both. This is consistent across plots for these tests.

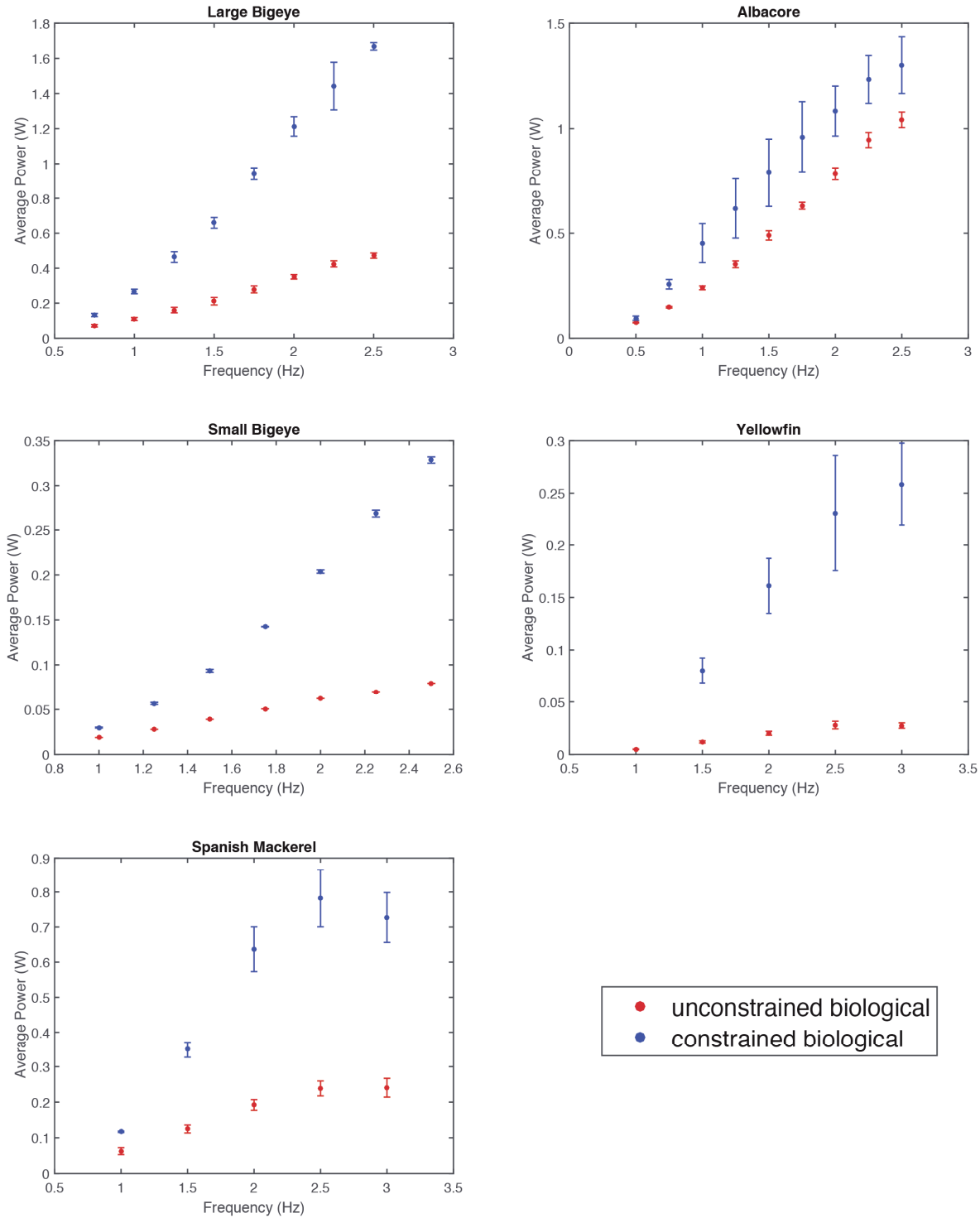

Figure 4.3: The cycle averaged power of the samples plotted against frequency.

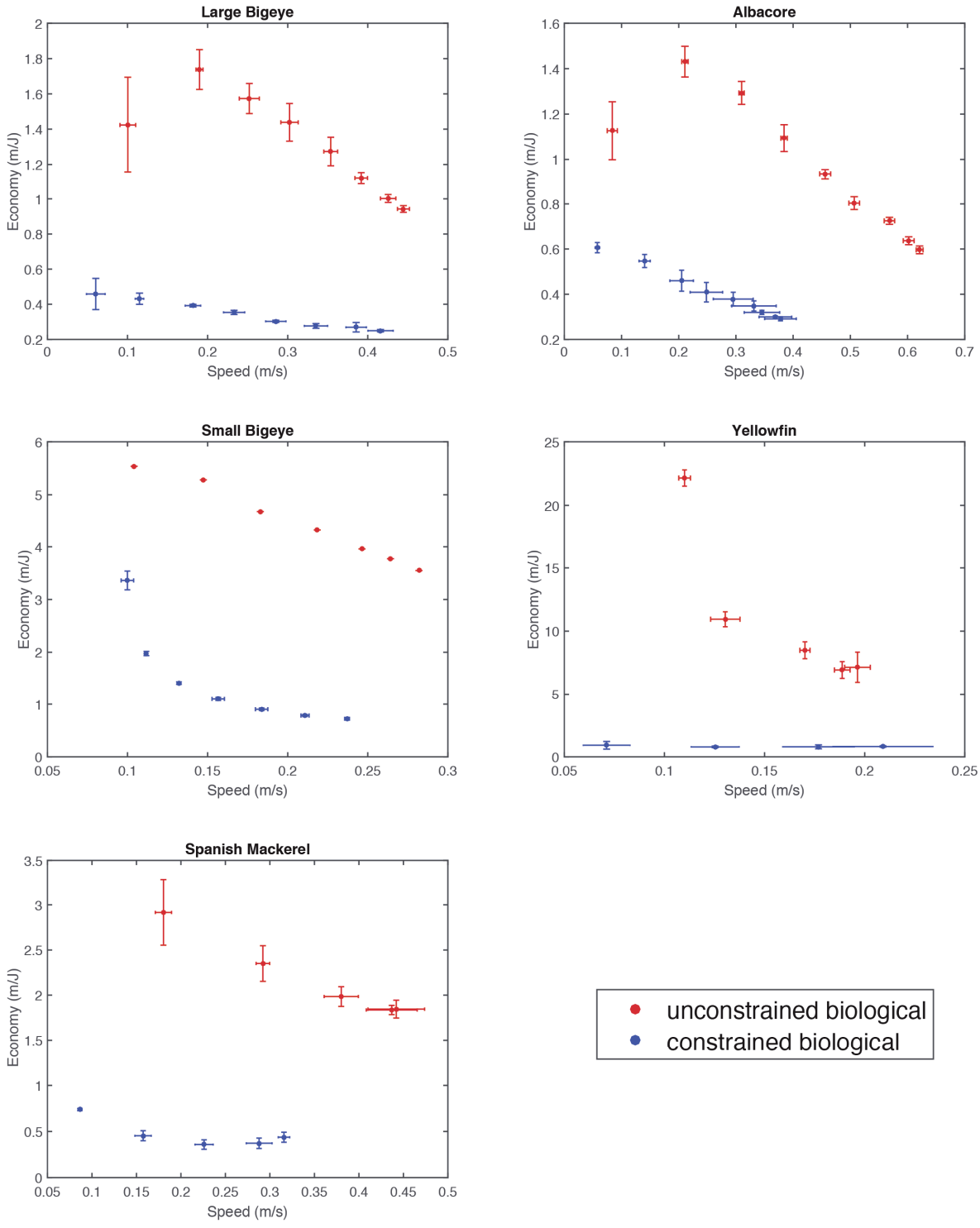

Figure 4.4: Free-swimming economy as a function of swimming speed. Note the peaks in the first two fins.

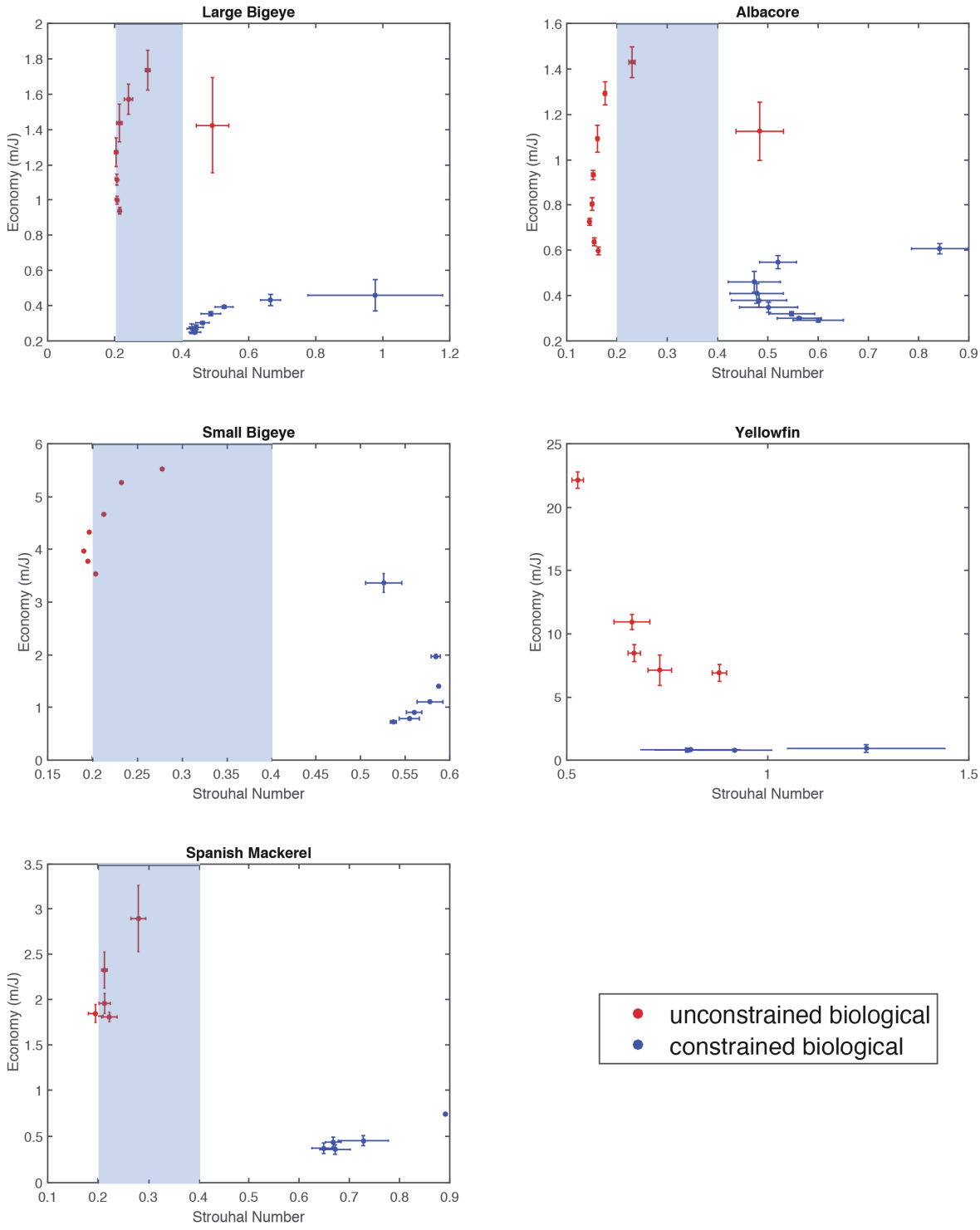

Figure 4.5: Free-swimming economy as a function of Strouhal number. The highlighted sections represent the known range of efficiency from St=0.2-0.4.

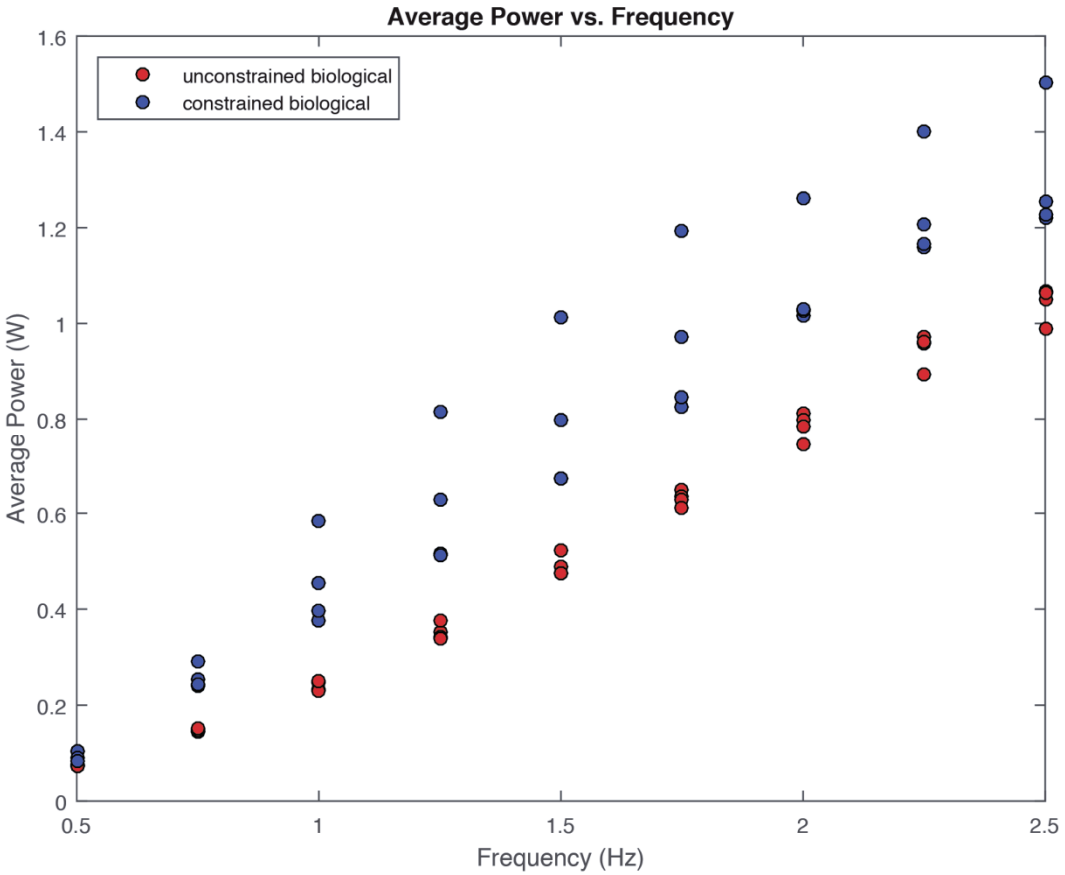

Figure 4.6: Average power for the albacore sample. The unconstrained tests are grouped tightly. The constrained tests are much more widely spread. This spread is correlated to the test set: the highest line of powers was the first set of constrained tests. Lower lines correspond to later test sets. This is likely a result of the strut used to constrain the fin being knocked loose at 2 Hz during the first set of testing, as seen by the dip in power above.

Chapter 5

Experiment: Artificial Peduncle

The experiments with the biological samples clearly illustrated the importance of the peduncle in high performance. They also suggest that speed and power are decoupled in some way, which is intriguing because it opens up the possibility of controlling each separately in an artificial system. If varying the "levels of constraint" at the peduncle varies performance—as was the case in the previous experiments—then there could be a way to tune the peduncle to maximize speed and minimize power. The purpose of these experiments is to formally characterize how different "levels of constraint" change performance, while simultaneously evaluating the performance of an artificial peduncle. There are several different ways to quantify "levels of constraint." The movement of the peduncle could be constrained in the sense that it takes more force to move it, i.e. the joint is stiffer. It could also be constrained in the sense that it has limits on its maximum bend angle. It is hypothesized that stiffness primarily influences power: as stiffer peduncle will increase power over a more compliant one, while bend angle primarily affects free-swimming speed: larger bend angles will increase speed over smaller bend angles. Each of these parameters was tested in isolation to determine its effect.

5.1 Experimental Setup

5.1.1 Artificial Peduncle

Manipulating the stiffness and bend angle required the creation of an artificial peduncle. In addition, ongoing biological testing, while a necessary and important step in this process, is not sustainable. Biological tissue must be kept on ice, it eventually breaks down and decays, and obtaining samples suitable for testing can be difficult. It is generally problematic to work with. An artificial system with careful repeatability that can replicate the peduncle is much more desirable.

The design of the peduncle went through several iterations before settling into the one used here. The first design consisted only of a single bearing wrapped in a silicone "skin" to mimic the peduncle and any inherent stiffness. This design did not perform well, so mechanical stops at the limits of bending were incorporated into subsequent designs. These mechanical stops mimic similar limits imposed by the spine of tuna. These designs, which were based on a living hinge concept, performed much better, but were fragile and did not lend themselves to easy manipulation of either stiffness or bend angle.

The final peduncle-caudal module used in this work is a combination of the previous designs (figure 5.1). The peduncle joint is modeled as a hinge at the leading edge of the caudal fin. Mechanical stops at either extreme limit the motion, and easily-swappable springs act as "tendons" to provide stiffness. Bend angle can be changed by swapping out the caudal fin piece of the module. The caudal fin itself is a rigid NACA 0020 airfoil to replicate the shape of the biological fins but not the flexibility. Though adding flexibility would increase the performance, it was not the focus of this work and was omitted. The caudal fin was designed to match the shape and size of a biological sample so that a mostly direct comparison could be made between the artificial and biological tests (the biological sample still has caudal flexibility).

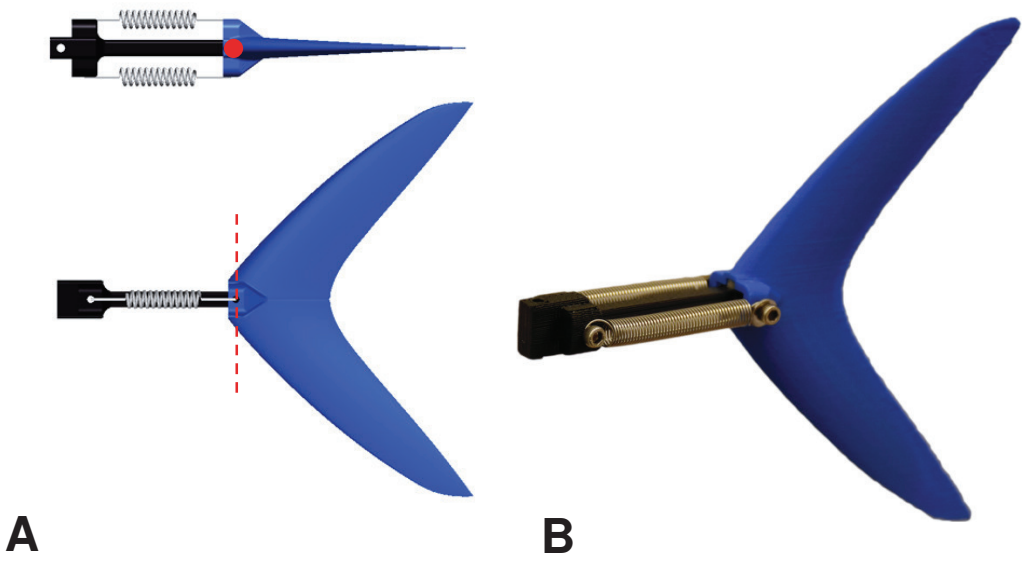

k (lbf/in)	0.26	0.43	1	1.5

Figure 5.1: The artificial peduncle design; A) Top and side view of the CAD model showing the swappable caudal fin (blue), the "backbone" that inserts into the tuna platform (black), and the replaceable springs. The dashed line in the side view and the red dot in the top view denotes the axis of rotation; B) The physical model.

5.1.2 Tuna Platform

The tuna platform replicates the kinematics of tuna swimming and was used in these tests to provide an increased level of biofidelity, allowing the experiments to account for body interactions, unlike many of the previously-discussed studies (figure 5.2). The platform replicates the motion of a tuna by using a two-node active tensegrity, a structure which has been previously used to study the kinematics of manta rays. The tensegrity is actuated by a drum located in the platform's 3D-printed plastic head, and is covered in a cast silicone skin. Two shafts stick up from the head: the first is a square bar which provides stability and keep the head stationary, and the second is a drive shaft connecting the actuation drum to the motor. This entire system fits into the rig, and testing procedure is no different than the isolated propulsors in the first experiment.

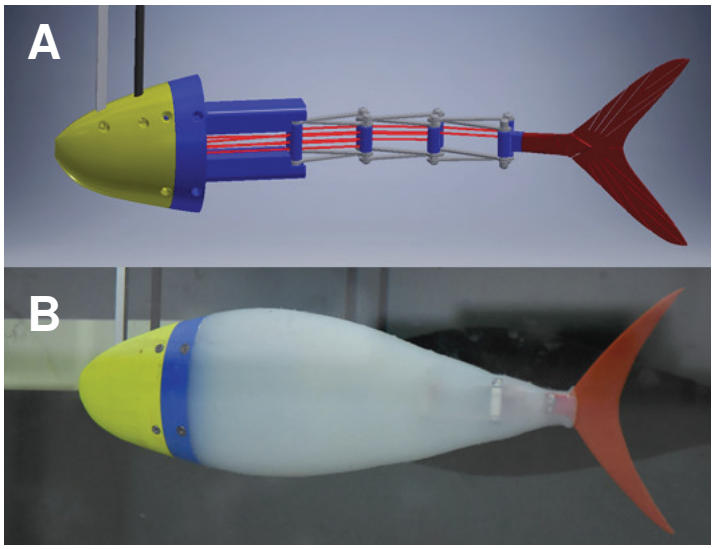

Figure 5.2: The tuna platform; A) CAD design of the tensegrity structure, courtesy of Jianzhang Zhu. There are three nodes, but the first is unused with just two necessary to replicate the tuna motion; B) The physical platform with the silicone skin.

The tuna platform does not have a permanent tail, but rather the last node of the tensegrity has a slot which accommodates the design of the artificial peduncle. This modularity allowed the numerous artificial peduncle and caudal fin designs to be quickly and easily swapped out and directly compared. The platform can even accommodate a biological tail (creating, if you will, a sort of "franken-fish") bonded to a fitted plastic piece.

The tuna platform measures 30 cm long from tip to the last node of the tensegrity; the tail modules used in these experiments add another 12 cm to the length. It is a maximum of 10 cm high and 6.5 cm wide. The platform is capable of producing deflections in excess of 60°.

5.1.3 Procedure

The procedure for these experiments again follows that in section 3.2. The nominal amplitude was set at 10°, although this value determined the amplitude of the motion of the drive motor. The tensegrity structure amplifies the input angle leading to total amplitude of approximately

30°. This amplitude matches the amplitudes observed in biology, and creates kinematics that are qualitatively very close to those of live tuna.

For the variable stiffness tests, six different stiffnesses were tested with a constant nominal maximum bend angle of 45 degrees. The first and last are not stiffnesses in the strict sense but correspond to zero stiffness (i.e. no springs) and infinite stiffness (i.e. a rigid peduncle). The remaining four values were chosen to provide a meaningful range given the forces acting on the system, from very compliant to fairly stiff. These four specific values can be seen in figure 4.1. The biological tail that was the basis for the artificial caudal fins was also tested. Videos were filmed for one test at each stiffness and frequency to provide kinematic data. The four tests that utilized springs will be referred to as the "spring tests" while the zero and infinite stiffness tests will be the "non-spring tests."

For the variable bend angle tests, three stiffnesses—zero, 0.26, and 1 lbf/in—were chosen to be additionally tested at a nominal maximum bend angle of 25°. These results, in comparison with the data at 45°, provide insight into the role of maximum bend angle.

5.2 Variable Stiffness: Results and Discussion

There are four important takeaways from these results. First, stiffness does seem to influence power without affecting speed (figures 5.3 and 5.4). Second and contrary to the hypothesis, increasing stiffness does not always increase power, but rather the behaviors of the stiffnesses are frequency dependent. Third, there are speeds that optimize economy for each spring stiffness (figure 5.5). Lastly, many of the Strouhal numbers fell within the high-efficiency range, though economy does not uniquely correlated to Strouhal number, corroborating the results of the biological experiments. A more in-depth discussion follows.

Varying Stiffness Affects Power but Not Speed

Figure 5.3 shows free-swimming speed plotted against frequency for each of the six stiffnesses and the biological sample. The results occupy two narrow bands. The biological sample and each of the spring tests tend to be tightly clustered, and the non-spring tests also appear together but at lower speeds. On the other hand, figure 5.4 shows the powers, which vary considerably. Looking only at the spring tests for example, the speeds range from 0.1753 m/s to 0.1877 m/s at 1.5 Hz, only a 6% difference. The powers, however, go from 0.09678 W to 0.1744 W, a 57% difference. These results corroborate the non-linear relationship between speed and power and indicate that stiffness can alter power without affecting speed drastically.

Frequency Dependence of Stiffness

Figure 5.4 plots all the data for average power vs. frequency, but the trends are frequency dependent. Figure 5.5 shows from power from 0 to 2 Hz. In this range power increases with increasing stiffness. Figure 5.6 shows power from a range of 2 to 3 Hz, and the trend in this range is reversed. There is a crossover point around 2.75 Hz, where the lower stiffness springs suddenly have a higher power than the higher stiffness springs.

Though the speed data is tightly grouped, there are crossover points that exist there as well. Within the upper band (the spring tests), the more compliant springs are faster at the lower frequencies, but the stiffer springs overtake them at the higher frequencies. The data points seem to invert between 1.5 and 1.75 Hz. The lower band of non-spring tests also has a crossover point, but the opposite trend. The infinite stiffness tests performed better at low frequencies with the zero stiffness tests overtaking them at about 2.5 Hz. Though these are two special cases and perhaps not directly comparable to the spring tests, this result is nevertheless unexpected because these cases

represent stiffness as it approaches its limits. How stiff or compliant can the springs be before the behavior changes? This result would seem to indicate that there must be at least some compliance or some stiffness or the speeds will suffer as a result.

As a final comment on speed, the biological sample does swim noticeably faster than the artificial fins at the higher frequencies. This is likely a result of fin flexibility. At low frequencies, deformations in the caudal fin would be minimal resulting in similar results to the rest of the spring tests. Higher frequencies increase these deformations increasing speed over that of the rigid caudal fin. The sudden drop at 3 Hz is because at that frequency for this fin, the rig began to vibrate, causing the bushings to lock up and resulting in an artificially low speed. If it had followed its own trend, it likely would have been very similar to the 1 lbf/in test at 3 Hz.

Certain Speeds Optimize Economy

Based on the speed and power plots alone, it is difficult to get a sense of the performance of each stiffness, because of how clustered the data is. Figure 5.7 makes it much more clear showing economy plotted against speed. Each stiffness peaks at a different speed, and there is not one stiffness with the highest economy for every speed. The compliant springs perform much better at lower speeds, while the stiffer springs perform the best at higher speeds. Overall economy is still quite low for the highest speeds, however. The artificial peduncle outperforms the biological tail over almost the entire range of speeds for a number of different stiffnesses. The highest economy is about 50% higher than the biological tail at the same speed (0.15 m/s). While this may not be the fairest comparison given that the biological sample is only a section of a long-dead fish, it is still encouraging that this passive model is capable of such improvements on the biological design, even without incorporating flexibility.

Several of the previously discussed works examined how the structural resonance of the foils affects swimming performance. Investigating the resonant behavior of the artificial peduncle was not a focus of this work, but based on the amplitude response of the fins, the two compliant springs reached a resonant frequency at about 1.75 Hz while the two stiffer springs did not exhibit resonant behavior. Rather interestingly, the zero stiffness case seemed to reach resonance at a higher frequency than the compliant springs—at 2.25 Hz. In any case, the peaks in economy do not occur at these structural resonances, nor do they seem to have any noticeable effect on the performance.

Strouhal Numbers fell in Expected Range, but the Metric is Not Unique for Economy

Figure 5.8 displays economy vs. Strouhal number. Many of the same trends as the first experiment are exhibited, but this time over half the data points fall in the 0.2 to 0.4 range, with a significant number of those points in a band at about St = 0.35. Once again, Strouhal number does not uniquely correlate with swimming performance when using a free-swimming metric, and the highest economies for each spring do not always correspond with Strouhal numbers in the expected range or at the lowest appearing Strouhal numbers.

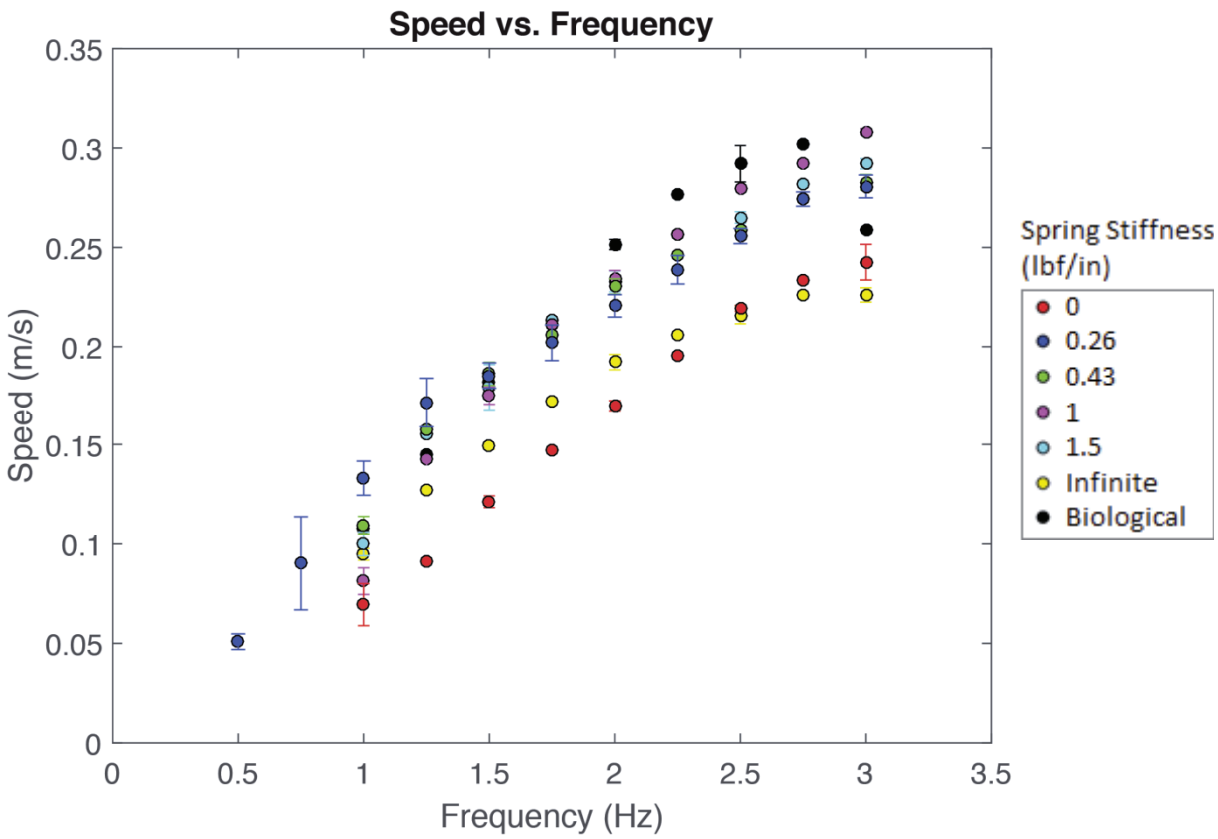

Figure 5.3: The results for speed as a function of frequency. The error bars reflect the standard deviations of 3 tests at each step of 0.5 Hz and 1 test at the intermediate 0.25 Hz to confirm the trends for every stiffness except 0.26 lbf/in which has 6 tests for each 0.5 Hz and 2 tests for the intermediate 0.25 Hz.

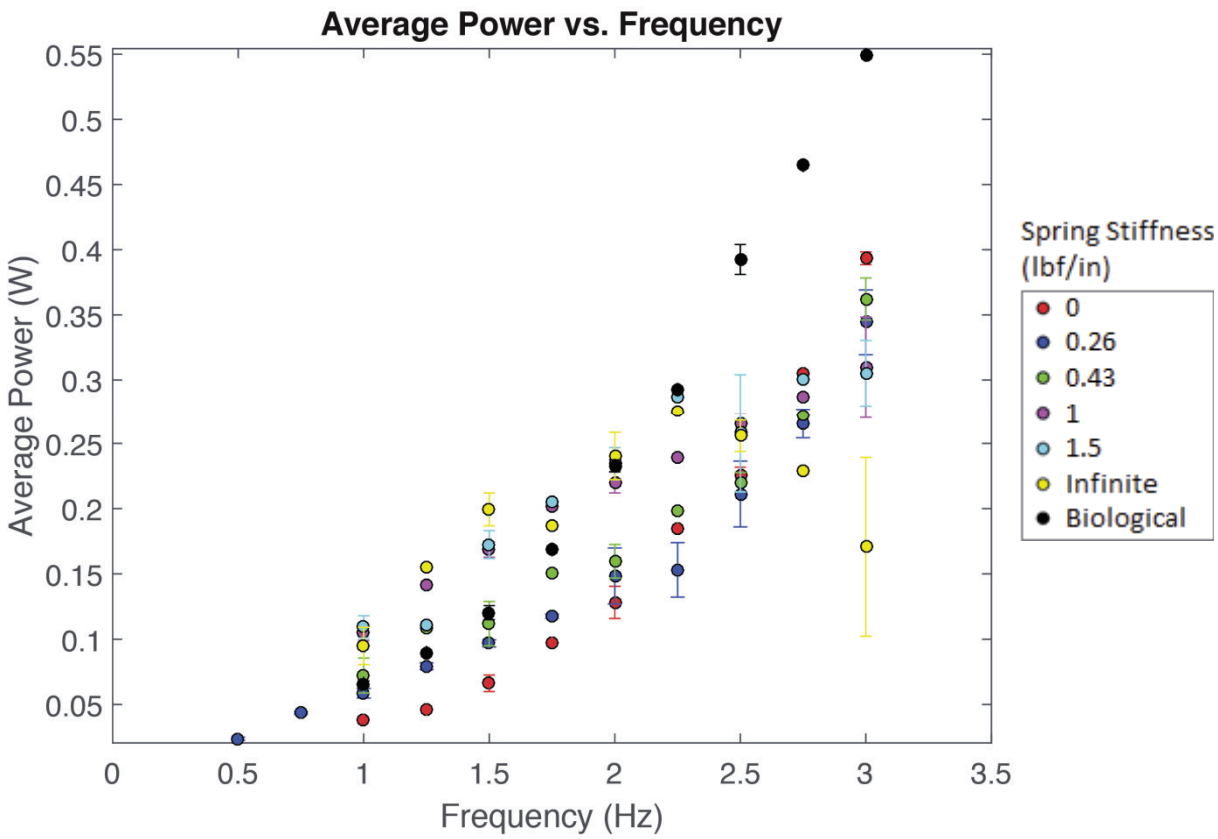

Figure 5.4: Average power plotted against flapping frequency.

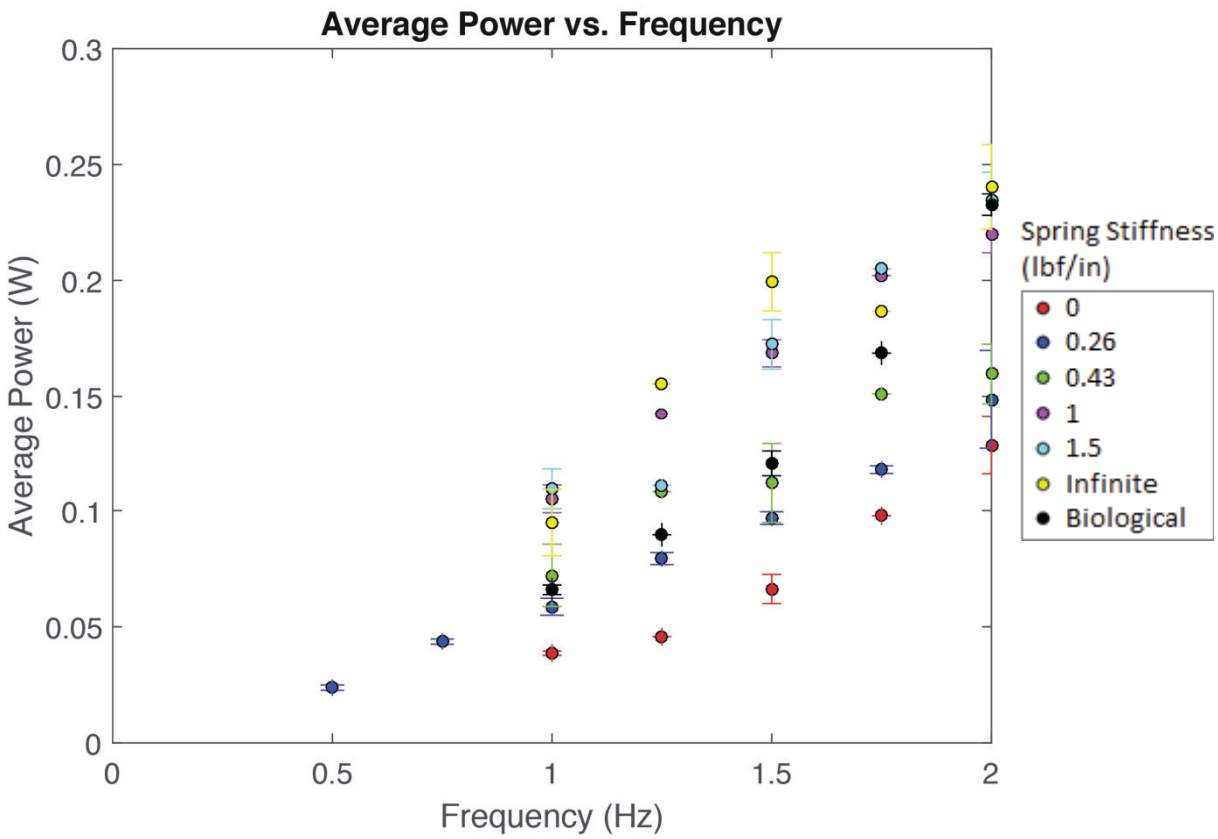

Figure 5.5: Average power at the lower frequencies.

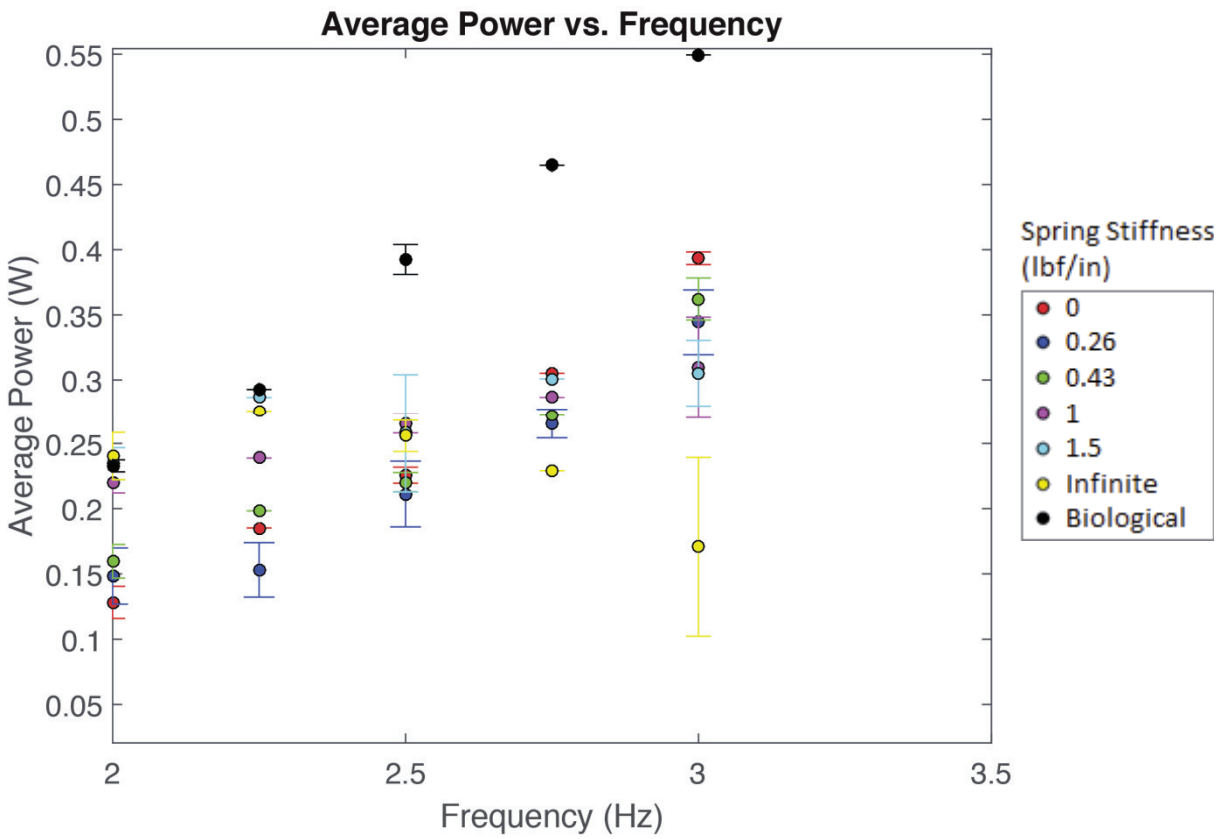

Figure 5.6: Average power at the upper frequencies.

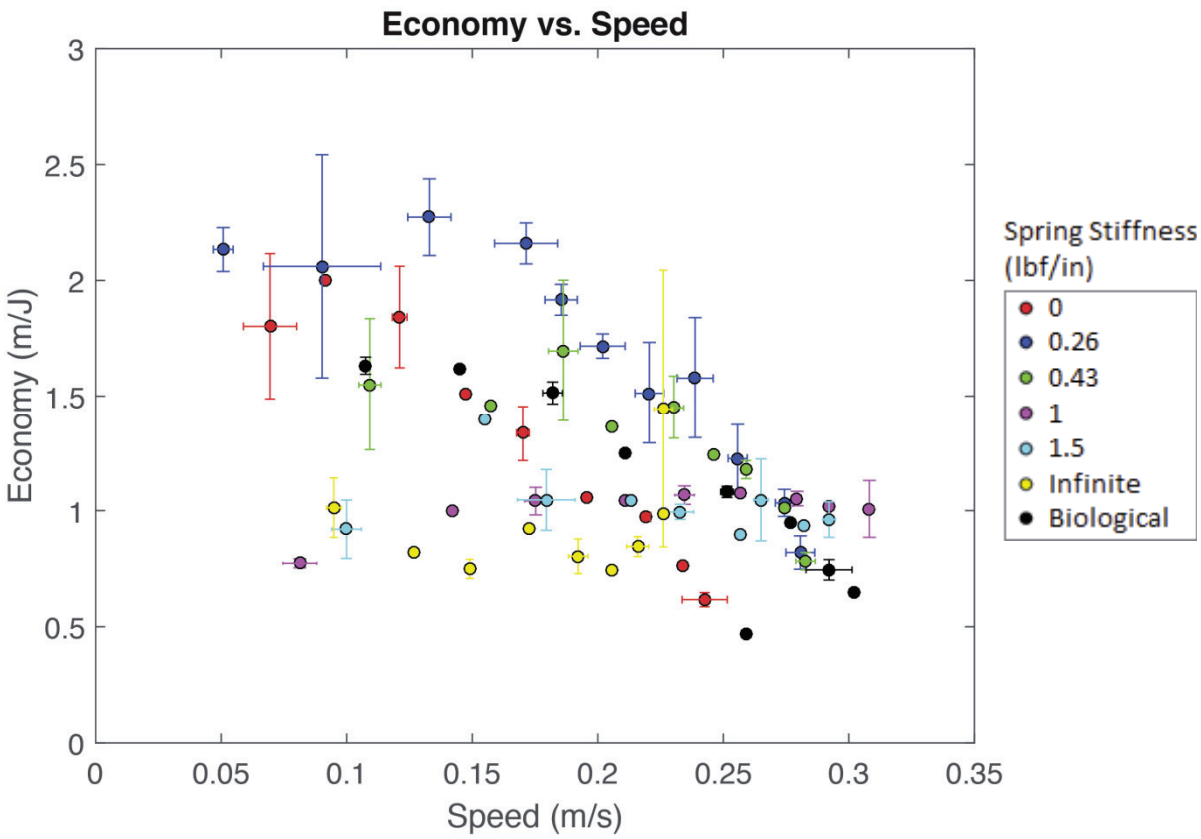

Figure 5.7: Free-swimming economy at the steady swimming speeds.

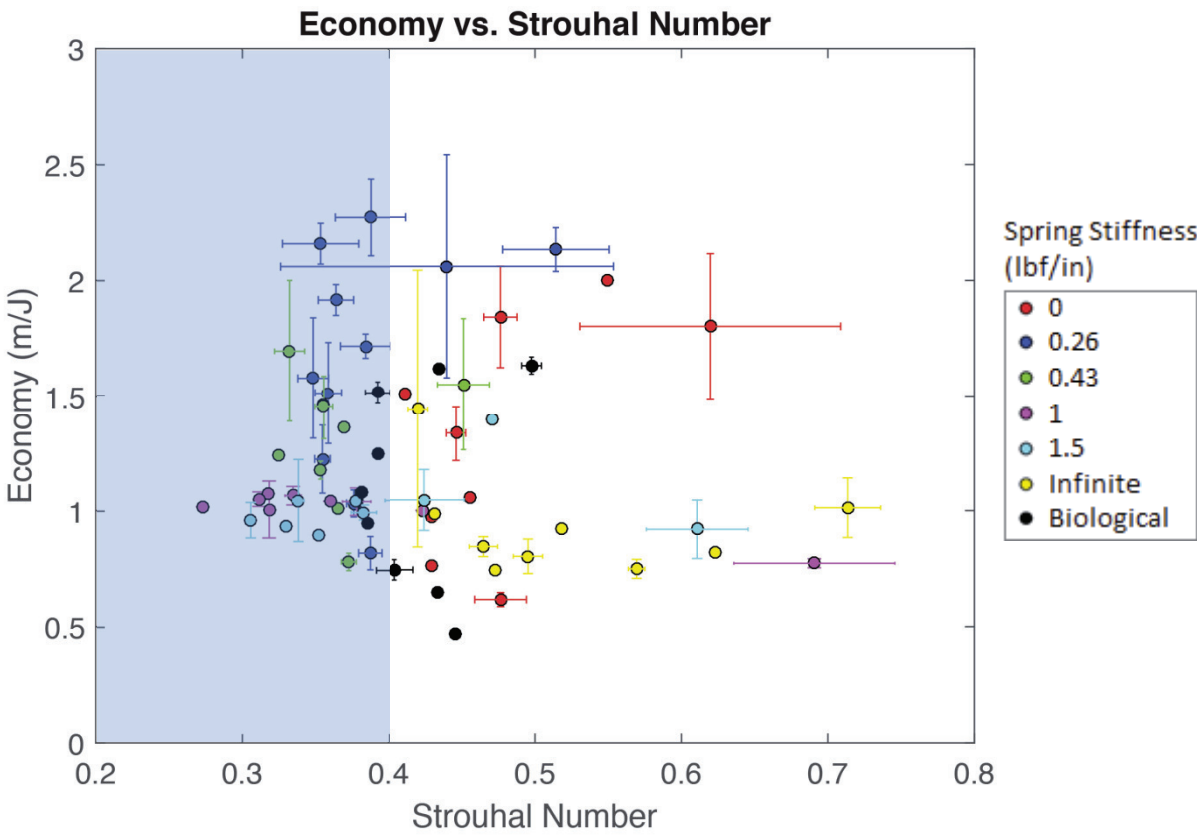

Figure 5.8: Free-swimming economy plotted against Strouhal number. The shaded region again represents the known high-efficiency range.

5.3 Variable Bend Angle: Results and Discussion

Having established the effect of stiffness on performance, the next stage was to vary bend angle and characterize its influence on performance. Three stiffnesses were chosen to be a representative sample of compliant to stiff: zero stiffness, 0.26 lbf/in, and 1 lbf/in.

5.3.1 Zero Stiffness Results

Figures 5.9a and 5.9b shows frequency plotted against speed and power, respectively, for both the 25 and 45 degree cases. The smaller bend angle increases the speed at all frequencies—by as much 35% at 2 Hz. However, it also increases power at all frequencies, so it is not obvious which bend angle is preferable. The plot of economy vs. speed (figure 5.9c) displays a very interesting behavior, showing the preferred angle is dependent on speed. At low speeds, the larger bend angle results in in higher economies, but as speed increases, the smaller bend angle is preferable, in one case increasing the economy by about 92% at almost identical speeds (approximately 0.23 m/s). As displayed in figure 5.9d, the Strouhal numbers have merely been shifted left, which is not unsurprising considering that a smaller bend angle would decrease the amplitudes, but many of the values are now within the 0.2 to 0.4 range. Once again there is not a one-to-one correlation between Strouhal number and economy.

5.3.2 0.26 lbf/in Results

The results for the 0.26 lbf/in stiffness showed many of the same trends as the zero stiffness tests. The speeds (figure 5.10a) are not universally increased, but a crossover does occur at about 1.5

Hz. The powers (figure 5.10b) are, however, increased across the range with the exception of 3 Hz, where the points are almost identical. The plot of economy vs. speed (figure 5.10c) once again yields a more complete picture. The smaller bend angle is again preferred at the higher speeds but the crossover is at a much later speed, and the gain in economy is not nearly as pronounced. Figure 5.10d shows economy plotted against Strouhal number. The 25 degree bend angle case displays a behavior not observed before in any of these tests. The Strouhal numbers expanded in both directions, for once displaying a one-to-one correlation. The highest economies, however, appeared at the highest Strouhal numbers and outside of the St = 0.2-0.4 range.

5.3.3 1 lbf/in Results

The results of the 1 lbf/in tests were unique. In theory, there should only be a significant difference at the higher frequencies. At low frequency, the stiff springs would keep the caudal fin from hitting the limits at the extremes. Their effect would only be seen at the higher frequencies when the forces become high enough to push the caudal fin into the mechanical stop, if that ever happens. The results should be fairly similar regardless, and they are. The speeds of the 25 degree case (figure 5.11a) appear higher, but only at one frequency (2 Hz) are the difference unquestionably statistically different. The powers for the 25 degree case (figure 5.11b) also appear lower, but again only the difference at 2.5 Hz is statistically significant. Figure 5.11c shows economy plotted against speed, and there is no crossover point: the 25-degree case outperforms the 45-degree case across the whole range of speeds, though only several of the points show statistically significant differences. The economy vs. Strouhal number plot (figure 5.11d) shows that the higher economies of the 25-degree case actually increased in Strouhal number with the exception of the low-economy, high-Strouhal number point off to the right of the clustered data.

5.3.4 Discussion

The existence of crossover points in the economies between the different bend angle cases in the first two stiffnesses seems consistent with the drag that would act on these fins. The zero stiffness fin exhibits very high bend angles over most of its flapping cycle. The crossover point for this stiffness occurs at a low speed, because as speed increases, drag increases, and it becomes increasingly beneficial to limit the area of the caudal fin that can cross into the free-stream. The crossover point for the 0.26 lbf/in stiffness occurs later because the bend angles only become high enough to matter at higher frequencies and thus higher speeds.

It would follow that for this system, the stiffest case of 1 lbf/in would show no crossover point or at least no significant difference between the two bend angles. The bend angles are simply not high enough for drag to matter. While most of the data points between the two cases are not statistically significant, it is noteworthy then that, for the few that are, the 25-degree bend angle performs better. Perhaps there is a more complicated interplay between thrust and drag production, or perhaps drag is not the driving force behind this behavior. However, given that there are so few significant differences between the two cases for this last stiffness, it is best to assume that these tests are inconclusive until further tests are conducted on the subject.

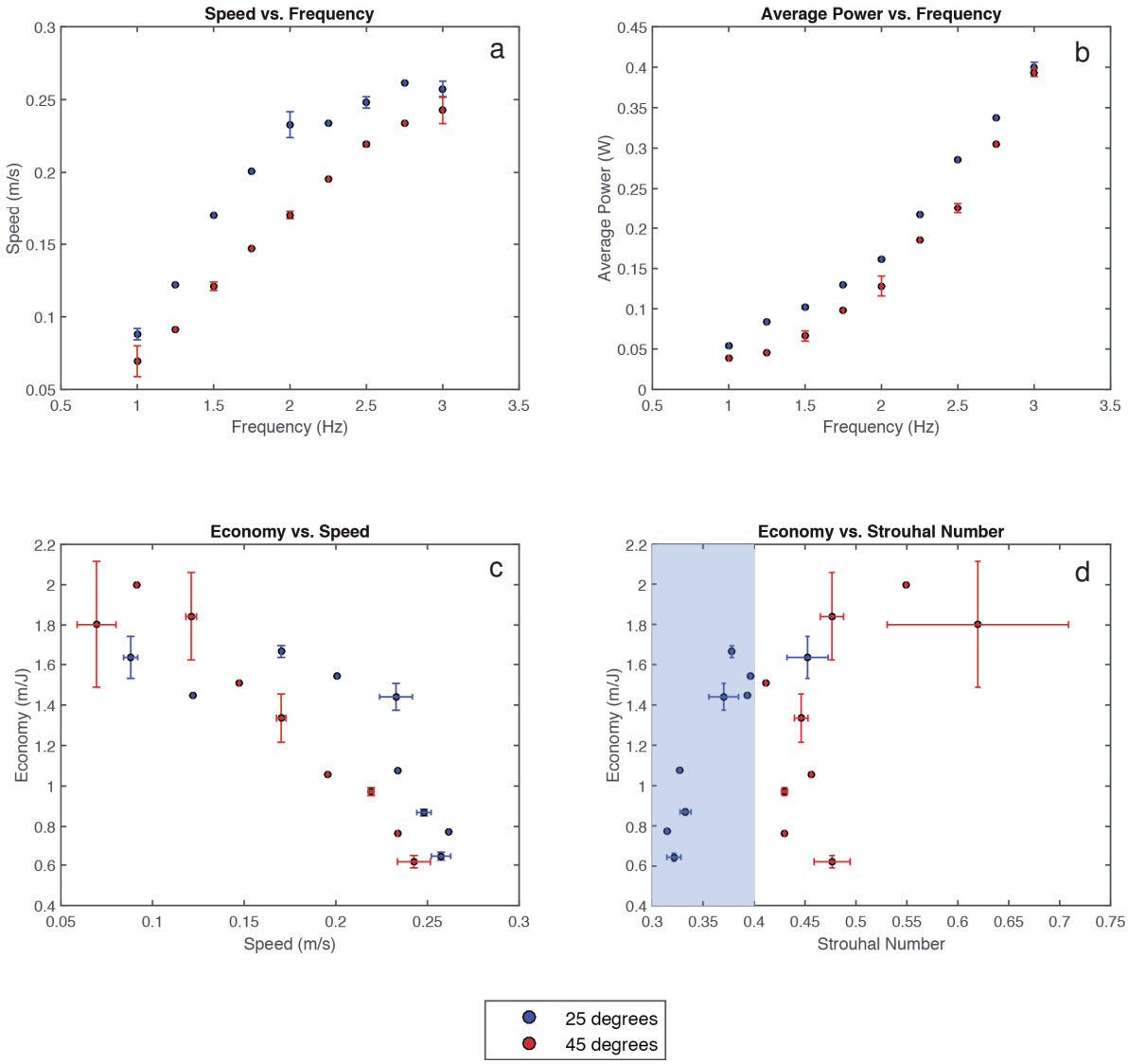

Figure 5.9: The results of the 25 degree bend angle for the zero stiffness test case.

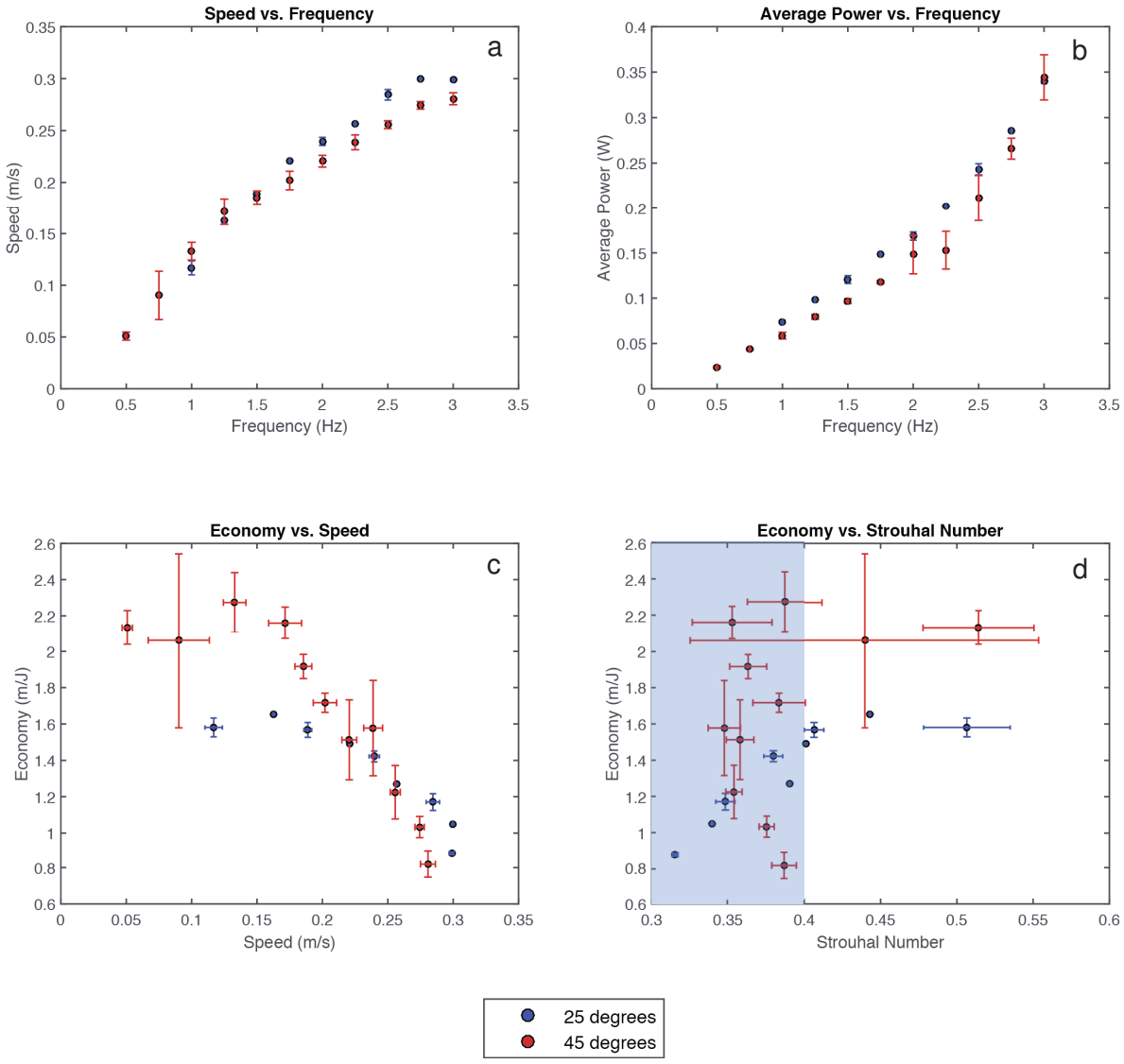

Figure 5.10: The results of the 25 degree bend angle for the 0.26 lbf/in stiffness test case.

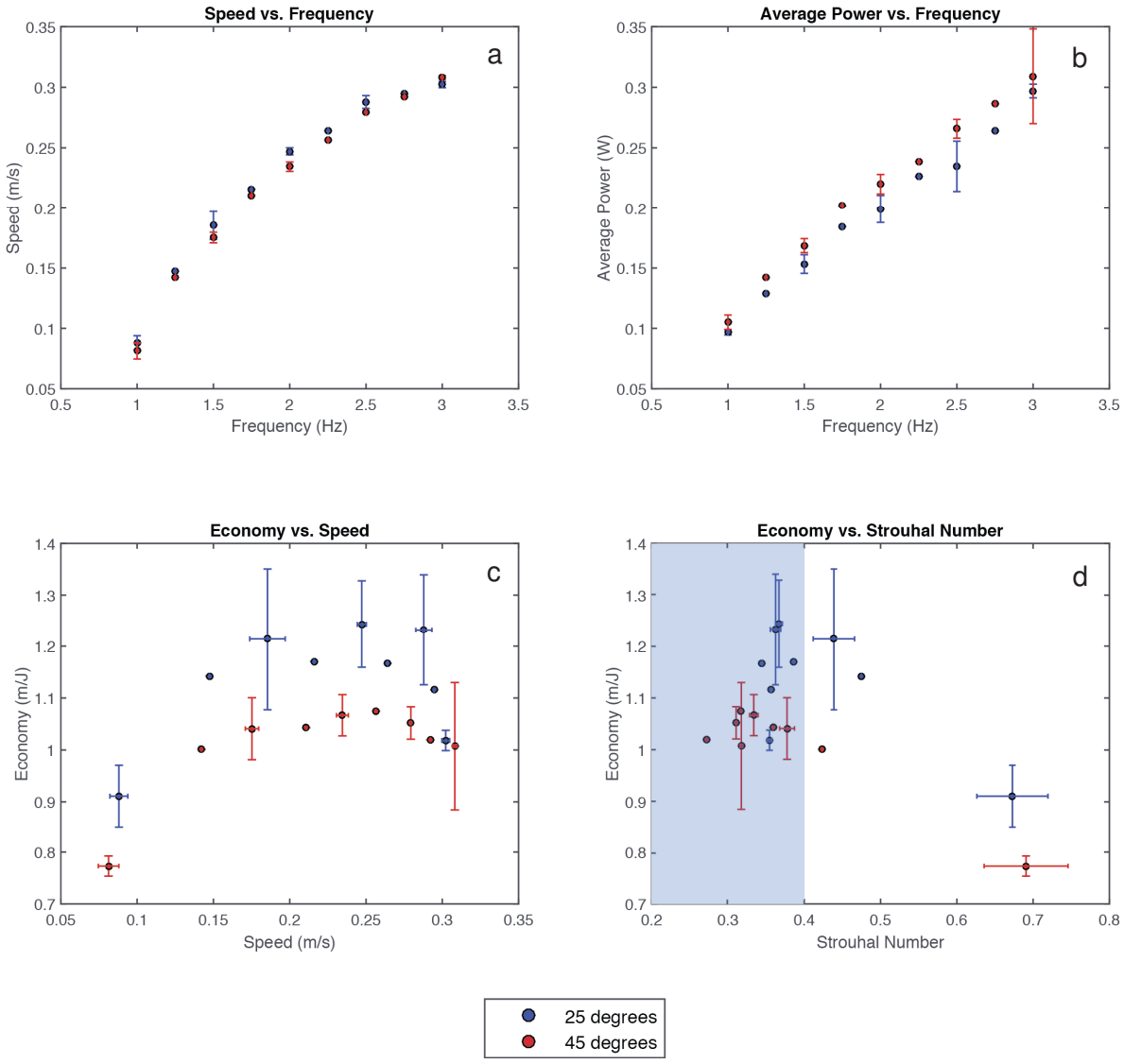

Figure 5.11: The results of the 25 degree bend angle for the 1 lbf/in stiffness test case.

5.4 Summary

It was hypothesized at the start of this chapter that the peduncle's stiffness and bend angle were the two most important factors in determining the performance of the peduncle. It was thought, based on differences in trends observed in the chapter 4, that the mechanisms controlling speed and power were decoupled: stiffness primarily influenced power while bend angle impacted speed. Only elements of this hypothesis were proven to be true.

The tests indicated that stiffness does control power. As stiffness was varied, the spring tests and the biological tests stayed within a fairly narrow band of speeds, while the power varied considerably. The economies of the various stiffnesses plotted against speed presents a much clearer picture of the overall behavior. Figure 5.12 presents the data as general trends. Each spring stiffness has a preferential speed at which the economy peaks. In addition, stiffer springs perform better than the more compliant ones at higher frequencies.

The bend angle influences speed and power—varying this angle changes both speed and power substantially. Taking results of both the bend angle and stiffness tests together, it would seem that limited motion is preferred as swimming speed increases. Stiffer springs and a smaller bend angle both performed better. Whether this is a function of drag or some other factor remains to be seen, but has clear implications in the design of a high-performing UUV. These results also inform the biological mechanism, providing strong evidence for the idea that tuna and other animals like them are actively controlling the stiffness of their tails, constantly tune them to optimize their own performance.

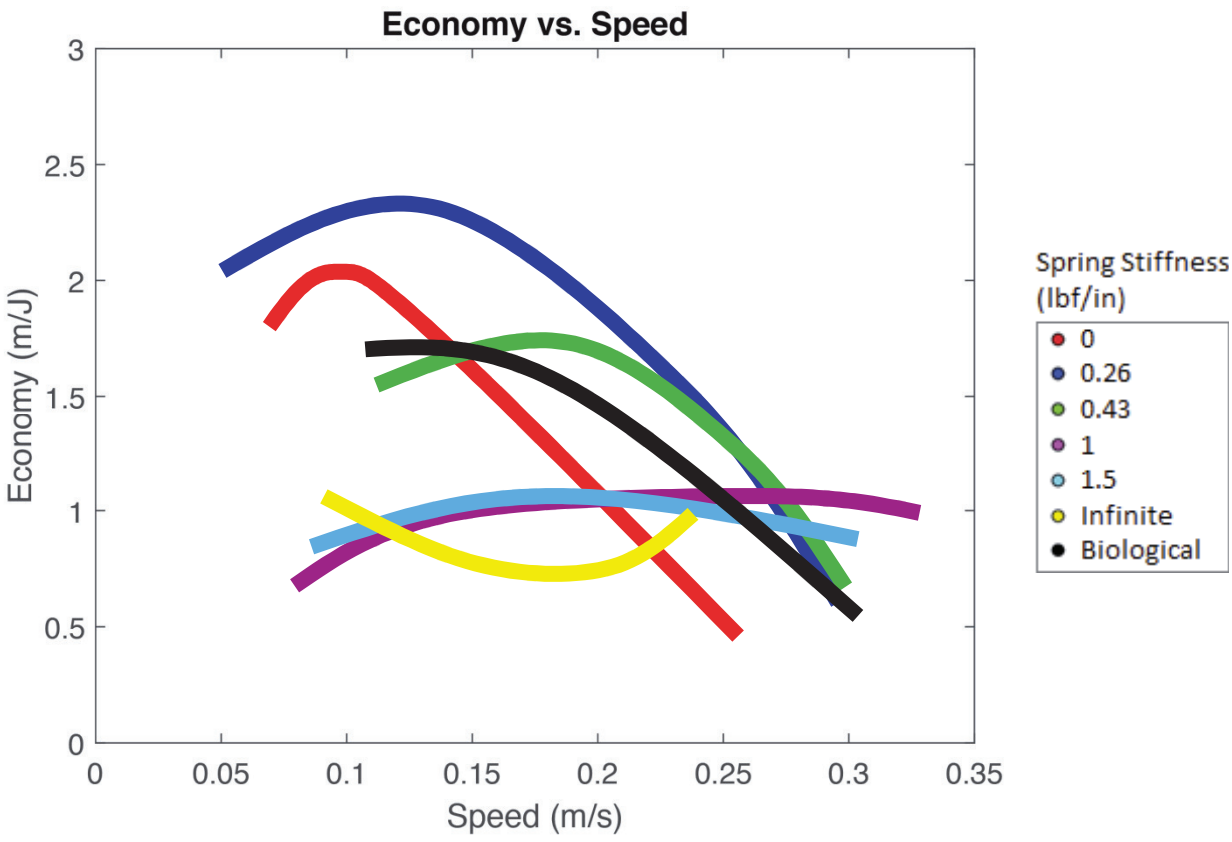

Figure 5.12: A representation of how economy varies with free-swimming speed. The curves are not fits of the data, but rather indicating the general trends that occur to make it easier to visualize.

Chapter 6
Conclusions

Tuna show significant promise as models for the next generation of UUVs. They are uniquely fast, economical, and maneuverable and offer levels of stealth beyond current technology. This work, however, is just one small aspect of the research necessary for designing an artificial tuna that even comes close to operating with the high-performance of the real fish.

This work had several aims: to measure the effect of the peduncle on performance in biological fins, to investigate the sensitivity of performance to specific characteristics of the peduncle, such as stiffness and bend angle, and to evaluate the performance of an artificial peduncle in comparison to a biological propulsor. The major contributions and findings are reviewed below.

6.1 Summary of Contributions

Free-swimming performance tests of biological samples showed that the peduncle undoubtedly enhances performance. The presence of an extra degree of freedom consistently increases speed and decreases power consumption across all the sizes and species tested. The results highlighted the existence of speeds which maximize performance and corroborated other's results that, although Strouhal number is a good indicator of performance as measured by efficiency, it is not a unique indicator of a free-swimming performance metric such as economy. The results of the biological tests also revealed a non-linear relationship between the speed and power of these fins.

That they are decoupled is promising for artificial systems, because it means each could be individually tuned to maximize performance, increasing speed while driving the power as low as possible.

These results informed the design and testing of an artificial propulsor in the next stage of experimentation. An artificial peduncle was designed to replicate the biomechanics of a tuna peduncle more closely than in previous studies and used a hinge joint at the peduncle and a rigid aerofoil tuna-like caudal fin to reproduce the kinematics of the tuna tail. The modularity of the design aided in the easy testing of several different joint stiffnesses and bend angles. The tuna platform also increased the biofidelity of the tests by providing a motion profile similar to thunniform swimming and allowed the inclusion of body interactions. Together, the tuna platform and artificial peduncle are a novel design for the modeling of thunniform swimming and the increased realism of the system only strengthens the assertion that the mechanisms observed here are comparable to those at work in biology.

Experiments on the artificial platforms showed that it is possible to tune performance by varying the stiffness and bend angle of the peduncle. In agreement with the initial hypothesis, varying the stiffness did affect power without changing the free-swimming speed significantly. However, contrary to the hypothesis, increasing flexibility did not always result in lower power consumption. Power (and to a smaller degree, speed) exhibited a frequency dependence. More compliant springs performed better at lower frequencies while stiffer springs overtook them at higher frequencies. Each spring also had a preferred speed which optimized economy and no spring had the highest economy over the whole range of speeds. The compliant springs had the highest economies at low speeds, and the stiff springs had the highest economies at higher speeds, though maximum economy was still quite low at the highest speeds.

Bend angle affected both speed and power, counter to the hypothesis that stated it would primarily influence speed. Comparing the economies of low and high bend angle cases for a given stiffness showed crossover points, with the smaller bend angle outperforming the larger one as speed increased.

Taking results of both the bend angle and stiffness tests together, it would seem that limited motion is preferred as swimming speed increases. Stiffer springs and a smaller bend angle both performed better at high speeds. Whether this is a function of drag or some other factor remains to be seen, but has clear implications in the design of a high-performing UUV. These results also inform The biological mechanism, providing strong evidence for the idea that tuna and other animals like them are actively controlling the stiffness of their tails, constantly tune them to optimize their own performance.

6.2 Future Work

There are many additional areas of research into tuna biomechanics and locomotion that both build off the research presented here and pursue topics that are not investigated.

Increasing the complexity of the measurement equipment and test rig would enable testing to continue in a similar vein, albeit with more a more robust and biofidelic system. This study was only concerned with the driving torque as a means of measuring power input to the fluid, but using a sensor capable of measuring torque and forces in all three axes could provide an increasingly complete picture of propulsor performance. Measuring thrust would also allow for measurements of Froude efficiency, providing another metric of performance to complement the free-swimming economy presented here. Several hardware improvements could be made to the test rig as well. Adding heaving capabilities in addition to the pitching already present would allow a wider range of motion profiles to be tested. Another degree of freedom could also be added to the test rig to enable

unimpeded motion in the xy-plane. The test allows motion in the streamwise direction to approximate free-swimming conditions, but another set of rails could be built to allow for cross-stream motion. The rig could also be made completely wireless to completely eliminate any outside forces that might bias the results.

The tuna platform provides a good model for testing, but it could also be changed or made more complex. The tests performed here do not include any fins, which do affect flow dynamics. The inclusion of fins could enhance performance by assisting in wake capturing. The tensegrity structure is only option for actuation, and it is limited in several respects. Tensegrities are inherently a complicated system to design, produce, and predict. It also produces monotonic motion, which is a fine approximation, but an approximation nonetheless. Micro-pneumatics and hydraulics are perhaps another viable option, and developing a system that could produce wavelike bending along the entire length of the body at varying amplitudes would increase the fidelity of the tuna platform.

The complexity of the peduncle-caudal fin model could be increased in various ways. Incorporating flexibility into the caudal fin should improve performance, but then necessitates the investigation of the coupling of peduncle and caudal flexibility. The peduncle itself could be modeled much more closely to the actual skeletal structure of tuna, using several small hinges or even going so far as to replicate the shapes of the bones themselves. This model was also entirely passive. With such strong evidence for variable stiffness in biology, a design for an artificial tuna peduncle capable of actively varying stiffness would be a worthy future direction, similar to the work Park et al. have done with dolphin peduncles.

Even without increasing the complexity or capabilities of these systems, this work provides an opportunity to reevaluate the results of prior research. Feilich and Lauder investigated the role of stiffness and caudal fin shape in pitching foils, but noted the lack of body as a shortcoming. The tuna platform and caudal-peduncle module enable similar tests to be performed on a system that is

much closer to that of biology. The work of Rosic et al. and others could be verified and updated similarly.

There are also computational fluid dynamics simulations that can be derived from these experiments. The video data can be reconstructed in three dimensions and simulated in CFD code to visualize the wake structures. The size and shape of the vortex rings could provide information about the performance on the most fundamental level: what fluid structures enable the higher performance of one stiffness over another? Once these fluid structures are known, a system can be reverse engineered to take advantage of them, being inspired by but not necessarily constrained by biology. The waveforms can also be used in simpler 2D pitching foil simulations, prescribing the kinematics and observing the wake structures that result.

Ultimately, the natural conclusion of this and all similar research is the creation of an autonomous vehicle the swims like a tuna. This work focuses on replicating the swimming motion, which is probably half of building an artificial tuna fish. The other half, which this work does not address in any way, is the replication of the biological sensory systems of tuna. Fish possess a lateral line which they use to sense flow; it informs their motion and allows them to capture wakes and vortices already present in a flow to reduce their power. Fully replicating a tuna fish would require the integration of sensing and motion in a processing and controls sense. While this might seem far off given the more fundamental nature of this work, it is research that could be conducted in parallel, to the eventual aforementioned goal.

Bibliography

Aleyev, Y. G. (1977). *Nekton*. The Hague: Junk.

Bandyopadhyay, P.R. (2005). Trends in biorobotic autonomous undersea vehicles. *IEEE Journal of Oceanic Engineering,* 30(1), 109-139.

Blickhan, R. & Cheng, J-Y. (1994). Energy storage by elastic mechanisms in the tail of large swimmers—a re-evaluation. *Journal of Experimental Biology, 168,* 315-321.

Colgate, J.E., & Lynch, K.M. (2004). Mechanics and control of swimming: A review. *IEEE Journal of Oceanic Engineering, 29*(3), 660-673.

Dewar, H. & Graham, J. (1994). Studies of tropical tuna swimming performance in a large water tunnel – energetics. *Journal of Experimental Biology, 192*(1):13-31.

Dewey, P. A., Boschitsch, B. M., Moored, K. W., Stone, H. A. & Smits, A. J. (2013).Scaling laws for the thrust production of flexible pitching panels. *Journal of Fluid Mechanics, 732*, 29-46.

Esposito, C.J., Tangorra, J.L., Flammang, B.E., & Lauder G.V. (2012). A robotic fish caudal fin: effects of stiffness and motor program on locomotor performance. *Journal of Experimental Biology, 215*(1), 56-67.

Feilich, K.L., & Lauder, G.V. (2015). Passive mechanical models of fish caudal fins: effects of shape and stiffness on self-propulsion. *Bioinspiration & Biomimetics, 10*(3).

Fish, F. E., & Rohr, J. (1999). Review of dolphin hydrodynamics and swimming performance. SPAWARS Tech Rep 1801. San Diego, CA.

Fish, F. E., Haj-Hariri, H., Smits, A. J., Bart-Smith, H., & Iwasaki, T. (2011). Biomimetic swimmer inspired by the manta ray. In Y. Bar-Cohen (Ed.), *Biomimetics: Nature-Based Innovation* (pp. 495-523). Boca Raton, FL: CRC Press.

Kasumyan, A. O. (2008). Sounds and sound production in fishes. *Journal of Ichthyology, 48*, 981-1030.

Kemp, T.(2014). Investigating Batoid-Inspired Propulsion: The Development, Testing, and Performance Analysis of a Tensegrity-Based Robotic Fin for Underwater Locomotion. Retrieved from http://libra.virginia.edu/catalog/libra-oa:6990.

Kishinouye, K. (1923). *Contributions to the Comparative Study of the So-called Scombroid Fishes*. Tokyo: The University of Tokyo.

Lucas, K.N., Thornycroft, P.J.M., Gemmell, B.J., Colin, S.P., Costello, J.H., & Lauder, G.V. (2015). Effects of non-uniform stiffness on the swimming performance of a passively-flexing, fish-like foil model. *Bioinspiration & Biomimetics,10*(5).

Moored, K. W., Dewey, P. A., Leftwich, M. C., Bart-Smith, H. & Smits, A. J., (2011). Bioinspired propulsion mechanisms based on manta ray locomotion. *The Marine Technology Society Journal, 45*(4), 110-118.

Moulton, J. M. (1960). Sounds and the schooling of fishes. *The Biological Bulletin, 119*, 210-223.

Park, Y-J, & Cho, K-J. (2013). Design and manufacturing a bio-inspired variable stiffness mechanism in a robotic dolphin. *Intelligent Robotics and Applications (Lecture Notes in Computer Science)* (pp. 302-309). Berlin: Springer.

Park, Y-J., Huh, T.M., Park, D., & Cho, K. (2014). Design of a variable-stiffness flapping mechanim for maximizing the thrust of a bio-inspired underwater robot. *Bioinspiration & Biomimetics, 9*(3).

Quinn, D.B., Lauder, G.V. & Smits, A.J. (2013). Scaling the propulsive performance of heaving flexible panels. *Journal of Fluid Mechanics, 738*, 250-267,

Rosic, M.N., Thornycroft, P.J.M., Feilich, K.L., Lucas, K.N., & Lauder, G.V. (2016). Performance variation due to stiffness in a tuna-inspired flexible foil model. *Bioinspiration & Biomimetics, 12*(1).

Shadwick, R.E., Rapoport, H.S., & Fenger, J.M. (2002). Structure and function of tuna tail tendons. *Comparative Biochemistry and Physiology Part A, 133*(4), 1109-1125.

Shelton, R. M., Thornycroft, P. J. M., & Lauder, G. V. (2014). Undulatory locomotion of flexible foils as biomimetic models for understanding fish propulsion. *Journal of Experimental Biology, 217*(12), 2110–2120

Sun, Q., Morikawa, H., Kobayashi, S., Ueda, K., Miyahara, H., & Nakashima, M. (2010). Structure and Bending Properties of Central Part of Tail Fin of Dolphin. *Journal of Biomechanical Science and Engineering, 5*(4).

Taylor, G. & Nudds, R. (2003). Flying and swimming animals cruise at a Strouhal number tuned for high power efficiency. *Nature, 425*(6959), 707-711.

Ziyu, R., Yang, X., Wang, T., & Wen, L. (2016). Hydrodynamics of a robotic fish tail: effects of the caudal peduncle, fin ray motions and the flow speed. *Bioinspiration & Biomimetics, 11*(1).